Published in final edited form as:
Adv Colloid Interface Sci. 2014 June ; 208: 76–88. doi:10.1016/j.cis.2014.01.004.

Dynamics and instabilities of lipid bilayer membrane shapes

Zheng Shi and **Tobias Baumgart***
Department of Chemistry, University of Pennsylvania, 231 S. 34th St., Philadelphia, PA 19104, USA

Abstract

Biological membranes undergo constant shape remodeling involving the formation of highly curved structures. The lipid bilayer represents the fundamental architecture of the cellular membrane with its shapes determined by the Helfrich curvature bending energy. However, the dynamics of bilayer shape transitions, especially their modulation by membrane proteins, and the resulting shape instabilities, are still not well understood. Here, we review in a unifying manner several theories that describe the fluctuations (i.e. undulations) of bilayer shapes as well as their local coupling with lipid or protein density variation. The coupling between local membrane curvature and lipid density gives rise to a ‘slipping mode’ in addition to the conventional ‘bending mode’ for damping the membrane fluctuation. This leads to a number of interesting experimental phenomena regarding bilayer shape dynamics. More importantly, curvature-inducing proteins can couple with membrane shape and eventually render the membrane unstable. A criterion for membrane shape instability is derived from a linear stability analysis. The instability criterion reemphasizes the importance of membrane tension in regulating the stability and dynamics of membrane geometry. Recent progresses in understanding the role of membrane tension in regulating dynamical cellular processes are also reviewed. Protein density is emphasized as a key factor in regulating membrane shape transitions: a threshold density of curvature coupling proteins is required for inducing membrane morphology transitions.

Keywords

Membrane fluctuation; Interleaflet friction; Membrane tension; Curvature instability; Protein density; Membrane shape transition

1. Introduction

Cellular membranes are highly dynamic and are a feature of the structural complexity of biological cells [1–3]. Membrane shape transitions are often coupled with specific functions of cellular compartments [4–6]. For example, remodeling of membranes, such as during vesicle budding [1,3,7] and membrane tubulation [8–11], is required for cellular signaling and cargo transportation. Thus, the diversity and dynamics of membrane shapes are vital for cell physiology [5].

*Corresponding author at: Department of Chemistry, University of Pennsylvania, 231 South 34th Street, Philadelphia, PA 19104, USA. Tel.: +1 215 573 7539. baumgart@sas.upenn.edu (T. Baumgart).

The lipid bilayer is the most fundamental structural component of biological membranes [12]. The physical properties of the bilayer have been extensively studied since the early 1970s [12–15], as a first step toward understanding complicated cellular membrane behaviors. The membrane's curvature elastic energy was found by Wolfgang Helfrich to play the major role in determining the shape of vesicles [14]. A large variety of experimentally observed shapes of red blood cells (RBC) can be nicely explained simply by minimizing the curvature elastic energy $F_{elastic}$:

$$F_{elastic}=\int \frac{1}{2}\kappa(C-C_s)^2 dA, \quad (1)$$

with appropriate constraints[16,17], where κ is the bending rigidity, C is the local mean curvature, C_s is the spontaneous curvature of the bilayer and A is the membrane surface area.

In Helfrich's spontaneous curvature model, the membrane is treated as a two-dimensional flexible film. While the model captures the essence of membrane geometries, the understanding of detailed, experimentally observed mechanical behaviors requires accounting for details of the membrane's bilayer architecture [18,19].

Equilibrium studies of membrane geometries revealed the underlying physics that contribute to cellular shapes. On the other hand, the mobility and shape transitions of cellular membranes are influenced by membrane dynamics. One of the most fundamental dynamic behaviors of a lipid bilayer is its fluctuations under thermal agitation. Analyzing the fluctuation spectrum can yield basic physical properties of the membrane and its interaction with the surrounding environment [20,21]. Another aspect of cellular dynamics involves the membrane deformation under external forces, which can be exerted either by solution flow [22,23] or through the interaction with the cytoskeleton [24,25]. Studies of membrane dynamics are able to disclose the spatiotemporal aspects of biological activities. For example, the motility of cells is usually driven by a cyclic generation and healing of membrane blebs or protrusions, with velocities ranging from 0.1 μm/min to over 10 μm/s [26–28].

There are many diseases in which membrane instability is believed to play a role. During fever, high body temperature induces RBC hemolysis and membrane fragmentation [29,30]. In Alzheimer's disease, altered membrane lipid composition is believed to cause an inherent tendency toward destabilization of cellular membranes [31,32]. More recently, the irreversible collapse of nuclear membrane envelopes was found to be responsible for massive DNA damage and tumor formation [33].

Leibler proposed in a theoretical study that membranes can become intrinsically unstable in a scenario where local membrane curvature and membrane composition couple [34]. However, these theoretical predictions have not been fully tested by experiments, due to the difficulties in quantifying membrane properties in or near unstable regimes.

Endocytosis is one of the best understood biological processes which potentially involve membrane curvature instabilities [35–37]. The formation of highly curved membrane structures is believed to be a result of the interplay between lipids and various peripheral proteins [3,38,39]. The mechanism by which proteins generate and stabilize/destabilize

membrane shapes, however, is still under debate. Understanding protein binding and assembling behaviors on membranes will serve as a starting point for explaining these processes.

The purpose of this contribution is to provide an overview of membrane shape dynamics and their coupling with protein–membrane interactions with an emphasis on the origin of curvature instabilities. We will begin with reviewing the basic concepts of thermal membrane fluctuations. Both conventional bending mode [20] and a more recently discovered slipping mode [21] are considered. Membrane tension as a result of constraining membrane fluctuations will also be reviewed. Curvature instability will be defined as the situation where fluctuation amplitudes grow divergently with time [34] and an instability criterion will be derived for a near-planar membrane. We will next discuss protein–membrane interactions and situations where proteins may induce curvature instabilities. Finally, we will suggest, from our perspective, several interesting directions and open questions in these areas.

2. Dynamics of membrane shape

2.1. Basic aspects of membrane shape fluctuations

Thermal out-of-plane fluctuations of membranes, also known as the “flicker phenomenon” [20], can be experimentally quantified through a variety of methods such as phase contrast microscopy [20], reflection interference contrast microscopy [40] or a recently developed optical tweezers method [41]. Recent reviews on this topic are available, see Refs. [42–44].

The free energy of a near-planar bilayer as determined by its curvature elastic energy can be written in the Monge representation [19,34,44],

$$F=\int \tfrac{1}{2}\kappa(\nabla^2 h)^2\,dxdy \quad (2)$$

where h denotes the height profile of the bilayer relative to the x, y plane (spontaneous curvature of the membrane is here neglected for simplicity).

The thermal average of the fluctuation amplitudes is connected with membrane properties through the equipartition theorem.

$$\left\langle |h(q)|^2 \right\rangle = \frac{k_B T}{A\kappa q^4} \quad (3)$$

A is the observed membrane surface area, and $h(q)$ and $h(r)$ are related through Fourier transform,

$$h(q)=\frac{1}{A}\int_A h(r)e^{i\vec{q}\cdot\vec{r}}\,d\vec{r} \qquad h(r)=\sum_q h(q)e^{-i\vec{q}\cdot\vec{r}}. \quad (4)$$

Thus, by measuring the spatial frequency spectrum at $q > \pi/L$ (when fluctuation wavelength is comparable to the size of the cell or vesicle L, this analysis is no longer accurate [20,45]), the membrane's bending rigidity κ can be determined.

The dynamics of membrane fluctuations is governed by the hydrodynamics of the surrounding solution through the Navier–Stokes equation for incompressible liquids:

$$\begin{gathered}\rho\frac{\partial\vec{v}}{\partial t}+\rho\left(\vec{v}\cdot\nabla\right)\vec{v}=\eta\nabla^2\vec{v}-\nabla p \\ \nabla\cdot\vec{v}=0.\end{gathered} \quad (5)$$

ρ is the density, v is the velocity, η and p are the viscosity, and the pressure of the enclosed fluid, respectively. For small amplitude motions discussed here, the nonlinear convective term $(v\cdot\nabla)v$ can be neglected [20,46,47].

If we consider a planar wave in the x-direction with wavenumber q_0, then the velocity and pressure of the liquid can be written as $v = v(z)e^{iq_0x+iwt}$, $p = p(z)e^{iq_0x+iwt}$ and the height of the membrane as $h = h_0e^{iq_0x+iwt}$. For simplicity, we will only consider the liquid below the membrane as illustrated in Fig. 1. However, it can be easily shown that a membrane with liquid on both sides will exhibit the same general behavior [46,48].

The solution of the equation of motion, assuming the liquid to be stationary at $z = -\infty$ is,

$$\begin{gathered}v_x=\left(iC_1e^{q_0z}+\frac{il}{q_0}C_2e^{lz}\right)e^{iq_0x+iwt} \\ v_z=\left(C_1e^{q_0z}+C_2e^{lz}\right)e^{iq_0x+iwt} \\ p=\frac{-iw\rho}{q_0}C_1e^{q_0z}e^{iq_0x+iwt}\end{gathered} \quad (6)$$

with $l^2=q_0^2+\frac{iw\rho}{\eta}$. C_1 and C_2 are constants and can be determined from the following boundary conditions at the bilayer–liquid interface:

$$\begin{gathered}T_{xz}|_{z=0}=\eta\left(\frac{\partial v_x}{\partial z}+\frac{\partial v_z}{\partial x}\right)\Big|_{z=0}=0 \\ T_{zz}|_{z=0}=P_z=-\frac{\delta F}{\delta h}\iff\left(2\eta\frac{\partial v_z}{\partial z}-p\right)\Big|_{z=0}=\kappa q_0^4h.\end{gathered} \quad (7)$$

$T_{ij} = -p\delta_{ij} + \eta(\partial_jv_i + \partial_iv_i)$ is the viscous stress tensor and P_z is the elastic restoring force due to membrane deformation. The first equation indicates there is no external force in the x-direction. The second equation describes the balance of forces in the z-direction, between liquid stress and the restoring force caused by membrane bending.

Continuity of the velocity at the membrane–liquid interface requires,

$$\frac{\partial h}{\partial t}=v_z|_{z=0}=(C_1+C_2)e^{iq_0x+iwt} \quad (8)$$

which is a first order approximation of the kinematic boundary condition $\frac{\partial h}{\partial t}=v_z|_{z=0}-\frac{\partial h}{\partial x}v_x|_{z=0}$ [49].

With $h = h_0 e^{iq_0 x + iwt}$ and the expressions for C_1 and C_2 obtained from Eq. (7), Eq. (8) leads to the dispersion relation:

$$w^2\rho^2 - \kappa\rho q_0^5 - 4iw\rho q_0^2\eta + 4q_0^4\eta\left(\frac{l}{q_0} - 1\right) = 0. \quad (9)$$

If we define unitless quantities: $S_0 = \frac{-iw\rho}{2\eta q_0^2}$ and $y = \frac{\kappa q_0 \rho}{4\eta^2}$, the dispersion relation becomes:

$$(S_0 - 1)^2 + y - \sqrt{1 - 2S_0} = 0. \quad (9')$$

The roots of the dispersion relation give the eigen frequencies of fluctuation modes. Since $y \ll 1$ (as will be discussed later), Eq. (9′) has two roots for a certain wave vector q_0, with the smaller one close to $S_0 = 0$ and the larger root close to $S_0 = 1 / 2$.

For $S_0 \sim 0$, one obtains the slow mode,

$$S_0 = y \Rightarrow w_1 = i\frac{\kappa q_0^3}{2\eta}. \quad (10)$$

In this case, the inertial term $\rho\frac{\partial \vec{v}}{2\eta}$ can be neglected while solving the Navier–Stokes equation (Stokes approximation). Eq. (8) then becomes $\frac{\partial h}{\partial t} = -\frac{\kappa q_0^3}{2\eta}h$ (this can be shown either by calculating a new general solution to replace Eq. (6) or by setting $\rho = 0$ in the expressions for C_1 and C_2). Assuming $h = h_0 e^{iq_0 x + iwt}$ leads directly to the slow dissipation mode $w = i\frac{\kappa q_0^3}{2\eta}$.

For $S_0 \sim 1 / 2$, we get the fast mode

$$S_0 \approx \frac{1}{2} \Rightarrow w_2 \approx i\frac{\eta q_0^2}{\rho}. \quad (11)$$

Numerical solutions for the slow and fast modes are shown in Fig. 2. It is worth noting that both modes are non-propagating since $exp(iwt)$ decays exponentially with time, indicating that the membrane is stable against perturbation [20]. Actually it is easy to see that when $y < y^* \sim 0.145$, there are always two real roots lying between $S_0 = 0$ and $S_0 = 0.5$ for Eq. (9′). This also means that for any wavenumber smaller than $q_0{}^* = 4\eta^2 y^*/\kappa\rho$, there are two pure imaginary values for the eigenfrequencies w, as shown in Fig. 2. Therefore, the membrane fluctuations will always exhibit two stable dissipating modes when $q_0 < q_0{}^*$.

Taking typical values for the bending rigidity, liquid viscosity and density: $\kappa \approx 10^{-19}$ J, $\eta \approx 10^{-3}$ Pa · s, $\rho \approx 10^3$ kg · m^{-3}, we have $y \approx 2.5 \times 10^{-11} \times q_0$. Since the upper cutoff for q_0 is defined by the spacing of lipids a_0 (about 1 nm) as $q_0 < \pi/a_0 \sim 10^9$ m^{-1} [20,50], this leads to $y < 0.025$. Thus, physically meaningful membrane fluctuations are always stable.

For the boundary condition Eq. (7), Brochard et al. [20] used $v_x|_{z=0} = 0$ instead of $T_{xz}|_{z=0} = 0$. If we assume the former boundary condition, the dispersion relation will be

$$w^2\rho-\kappa q_0^5\left(1-\frac{q_0}{l}\right)=0 \text{ or } S_0^2\sqrt{1-2S_0}+y\left(\sqrt{1-2S_0}-1\right)=0. \quad (9'')$$

For a certain $y < y^{**} \sim 0.155$ (or $q_0 < q_0^{**}$), Eq. (9″) also gives two dissipation modes between $S_0 = 0$ and $S_0 = 0.5$. As shown in Fig. 2, the dissipation modes resulting from two different boundary conditions behave very similarly. In fact, the two slow modes are indistinguishable; only the fast modes differ slightly without affecting the q_0^2 dependency. We note that both boundary conditions have been successfully applied to explain experimental data [20,21,34,51]. Only techniques with an extremely high tempo-spatial resolution would have the potential to identify the 'correct' boundary condition.

The foregoing discussion describes the dissipation of membrane fluctuations into the bulk liquid beneath the membrane. If both sides of the membrane are immersed in bulk liquid, the slow dissipation mode should be modified to $w=i\kappa q_0^3/4\eta$.

For a membrane in the vicinity of a substrate, the fluctuation spectrum of the membrane will be modified due to the presence of steric repulsion and van der Waals attraction between the membrane and substrate [46,47,51]. In biological systems, this substrate effect could be a result of membrane adhesion to the cell cortex, cytoskeleton, or to other surfaces [19,52–54].

In this case, the free energy of the membrane can be modified as follows,

$$F=\int\left\{\tfrac{1}{2}\kappa\left(\nabla^2 h\right)^2+V(z)\right\}dxdy \quad (2')$$

with $V(z)$ representing an effective interaction potential. In a harmonic approximation, the interaction potential can be approximated as $V(z) \approx \Omega h^2/2$, with $\Omega = d^2V/dz^2$ evaluated at the average position of membrane.

The velocity field of the liquid between the membrane and the substrate should be vanishing at the position of the substrate instead of at $z = -\infty$ as was used for deriving Eq. (6). Consequently, the dispersion relation of a fluctuating (monolayer) membrane at a distance l_0 from the substrate becomes (only the slow mode is considered) [51],

$$w=i\frac{\kappa q_0^4+\Omega}{\eta q_0}\frac{\sinh^2(q_0l_0)-(q_0l_0)^2}{\sinh^2(q_0l_0)-(q_0l_0)^2+\sinh(q_0l_0)\cosh(q_0l_0)+(q_0l_0)}$$
$$\rightarrow w=\begin{cases} il_0{}^3\frac{\kappa q_0^6+\Omega q_0^2}{\eta}, (q_0l_0 \ll 1) \\ i\frac{\kappa q_0^4+\Omega}{2\eta q_0}, (q_0l_0 \gg 1). \end{cases} \quad (10')$$

Once the dispersion relation is obtained, the power spectrum of membrane undulations can be calculated from the fluctuation dissipation theorem. It can be shown that the power spectrum is entirely dominated by the slow mode [20,34]. Thus, for the following discussion, we will focus on the slow mode only.

2.2. An additional dissipation mode as the result of inter-leaflet friction

2.2.1. General theory—As discussed above, membrane shape fluctuations are influenced by the membrane's bending rigidity and therefore Eq. (10) is also called the 'bending mode' of dissipation [2,21,55]. A second way of damping membrane fluctuations takes into account the double-leaflet structure of the lipid bilayer [19,21,56]. Local membrane bending generates a lipid density difference between the two monolayers, a process which can be damped by the friction in the tail region of the hydrocarbon chain while two monolayers are sliding over each other [19]. As will be shown below, the presence of inter-leaflet friction will change the fluctuation spectrum and give rise to an additional dissipation mode. This effect is more pronounced when two leaflets are intrinsically asymmetric [8], which is biologically significant since peripheral proteins as well as lipids are known to distribute asymmetrically across the plasma membrane [57].

Consideration of the lateral redistribution of lipids leads to the following modified free energy expression,

$$F=\int\left\{\tfrac{1}{2}\kappa\left(\nabla^2 h\right)^2+\tfrac{1}{2}k\left[\left(\rho^{+}+d\nabla^2 h\right)^2+\left(\rho^{-}-d\nabla^2 h\right)^2\right]\right\}dxdy. \quad (12)$$

k is an elastic area compressibility modulus, d is the distance between the mid-surface of the bilayer and the neutral surface of a monolayer, $\rho^{\pm}$ is the scaled deviation of lipid density from its equilibrium value, and '+' and '−' represent the outer and inner leaflet respectively. In the presence of the interaction potential $V(z)$, additional modifications of the membrane fluctuation spectra are thoroughly discussed in Ref. [47].

Dynamics of the liquid on both sides of the membrane are still determined by the Navier–Stokes equation but the balancing of forces at the boundary (Eq. (7)) is altered by the lateral redistribution of lipids. The modified boundary conditions are [21],

$$\begin{aligned}\pm T_{xz}^{\pm}|_{z=0}&=\nabla\left(\tfrac{\delta F}{\delta\rho^{\pm}}\right)-\mu\nabla^2 v_x^{\pm}\big|_{z=0}\pm b_f\left(v_x^{+}-v_x^{-}\right)\big|_{z=0}\\ -T_{zz}^{\pm}|_{z=0}+T_{zz}^{-}|_{z=0}&=P_z=-\tfrac{\delta F}{\delta h}=-\tilde{\kappa}q_0^4 h+2kq_0^2\rho d.\end{aligned} \quad (13)$$

The first equation displays the balancing of forces in the x-direction, between the viscous stress of 3D liquid motion and the 2D forces on membrane: surface pressure gradient, viscous stress in the membrane and inter-leaflet friction, where μ is the membrane viscosity and b_f is the inter-leaflet friction coefficient. The second equation describes the balancing of forces in the z-direction. Here, $\tilde{\kappa}=\kappa+2d^2k$ describes the renormalization of bending rigidity by the effect of elastic stretching and compression, ρ is defined as $\rho\equiv(\rho^{+}-\rho^{-})/2$, representing the density difference between two monolayers.

The equation of motion is determined by the continuity of velocity $\partial h/\partial t=v_z|_{z=0}$, and lipid density $\partial\rho^{\pm}/\partial t=-\partial v_x^{\pm}/\partial x|_{z=0}$. Solving Eq. (5) with the new boundary conditions and applying the Stokes approximation to get the expressions for v_x and v_z, yields the following equation of motion for the membrane:

$$\frac{\partial}{\partial t}\begin{pmatrix} h \\ \rho \end{pmatrix} = -M\begin{pmatrix} h \\ \rho \end{pmatrix} = -\begin{pmatrix} \tilde{\kappa}q_0^3/4\eta & -q_0 kd/2\eta \\ \dfrac{kdq_0^4}{2b_f+2\eta q_0+2\mu q_0^2} & \dfrac{kq_0^2}{2b_f+2\eta q_0+2\mu q_0^2} \end{pmatrix}\cdot\begin{pmatrix} h \\ \rho \end{pmatrix}. \quad (14)$$

The two eigenvalues of the dynamical matrix M, γ_1 and γ_2, represent two dissipation modes of the membrane fluctuation ($\gamma = -iw$); these are shown in Fig. 3 for a typical set of membrane parameters. In order for the membrane to be stable, $\gamma_{1,2}$ should be larger than zero so that $exp(-\gamma t)$ will decay with time. This leads to $\tilde{\kappa} \geq 2d^2k$, which is always true considering $\tilde{\kappa} = \kappa + 2d^2k$ and κ is positive. Thus, lateral redistribution of lipids only provides an alternative way to damp membrane fluctuations; the linear stability of the bilayer with respect to perturbation is not altered. Since the system has three degrees of freedom (h, ρ, $\bar{\rho}$), where $\bar{\rho} \equiv (\rho^+ + \rho^-)/2$ is the average lipid density, there is a third dynamic mode corresponding to $\bar{\rho}$. However, it is easy to see that fluctuation of $\bar{\rho}$ is decoupled from the other two degrees of freedom and therefore won't influence the shape of the membrane [21,58].

At small q_0, expanding about $q_0 = 0$ the expressions for γ that result from Eq. (14) gives $\gamma_1 = \frac{kq_0^2}{2b_f}$ and $\gamma_2 = \frac{\kappa q_0^3}{4\eta} \cdot \gamma_2$. γ_2 corresponds to the damping of the conventional bending mode via the surrounding liquid. It differs from Eq. (10) by a factor of two, which is due to the fact that we only considered the liquid on one side of the membrane in deriving Eq. (10). γ_1 is a new 'slipping mode' which describes the damping of inhomogeneous lipid density by inter-leaflet friction. At large q_0, $\gamma_1 = \frac{\tilde{\kappa}q_0^3}{4\eta}$ and $\gamma_2 = \frac{k\kappa}{\mu\kappa}$; here, γ_1 becomes the rate for dissipation in the surrounding liquid, with an effective bending rigidity $\tilde{\kappa}$. The increase of the effective bending rigidity is due to the inability of lipid density to respond as fast as the decay rate of height fluctuations [21]. In this regime, the dissipative mechanism for γ_2 is related to the properties of the 2D membrane, which changes from inter-leaflet friction to the membrane viscosity.

A number of studies have contributed to the measurement of the inter-leaflet friction coefficient b_f [8,21,56,59–61]. The results vary largely for different systems, from 2.7×10^7 up to 3×10^9 J · s · m^{-4}, making it hard to estimate the contribution of interleaflet friction. Here, we take the result from the most recently developed experimental technique [60], where b_f was measured as 3×10^9 J · s · m^{-4} for an unsupported bilayer and found to be independent of lipid chain length. Taking typical values for the physical constants: $\kappa \approx 10^{-19}$ J, $k \approx 7 \times 10^{-2}$ J · m^{-2}, $\eta \approx 10^{-3}$ Pa · s, we find that γ_2 is comparable to γ_1 at around $q_0 = 0.5$ μm^{-1}. For smaller wavelengths ($\lambda < 1$ μm), the dominating pathway for dissipation begins to be controlled by membrane properties instead of the bulk liquid viscosity. For the membrane viscosity μ, recent measurements have obtained $\mu \approx 10^{-9}$ J · s · m^{-2} for a liquid disordered phase and $\mu \approx 10^{-8}$ J · s · m^{-2} for a liquid ordered phase [62], consistent with earlier measurements [59,63]. Thus, the contribution from membrane viscosity can usually be neglected compared to interleaflet friction considering $\mu q_0^2 < b_f$ for $q_0 < 10^9$ m^{-1}.

The additional dissipation mode discussed above has been confirmed both by molecular dynamics simulations of a coarse-grained (CG) bilayer model [55], and by flicker spectroscopy studies of the fluctuation spectrum of giant vesicles [61]. The simulation observed a double-exponential decay of the fluctuation, with decay rates nicely agreeing with the predicted values for γ_1 and γ_2 [55]. The experimental fluctuation spectra were found to systematically deviate from the pure-bending behavior at large wavenumber and the relaxation rates of the fluctuation clearly obeyed $\sim q_0^2$ [61]. These findings directly support the existence of the slipping mode and the crossover of the dominating dissipation mode from bending to slipping as q_0 increases.

It should be noted that, in the above discussions, a number of simplifying assumptions were made. For example, the overall (average) geometry of the membrane was not considered beyond a planar geometry, the magnitude of fluctuations was assumed to be small, and membrane shear dissipation was neglected. These simplifications, while valid in most cases, do not capture certain phenomena that occur in special situations. For example, membrane shear viscosity becomes essential in highly curved membrane tethers [58]. It is also likely that the presence of peripheral proteins on the bilayer can greatly enhance the shear viscosity of the membrane. A model regarding the complex dynamic behaviors of biological membrane without making most of these simplifications is discussed numerically in a recent paper [58], illustrating new and nontrivial dynamics of lipid membranes.

2.2.2. Chemically triggered membrane undulations experimentally confirm the presence of the 'slipping mode'—Besides the above-mentioned flicker spectroscopy study [61], the slipping mode of bilayer was revealed in experiments that involved local delivery of a basic pH solution to giant vesicles. In these experiments, upon the arrival of chemicals at the vesicle surface, Fournier et al. observed a large-amplitude undulation of the membrane followed by ejection of membrane tubules [5,8,64,65]. In interpreting these observations, the basic solution was assumed to increase the repulsion between lipid head groups, thus locally decreasing the lipid density of the outer monolayer. By measuring membrane undulations under chemical modification, one can test the coupling between lipid density and bilayer shape which is controlled by inter-leaflet friction as discussed in the preceding section.

Consider that, at time zero, the basic chemical reduces the equilibrium lipid density of the outer leaflet by ε. The free energy of the bilayer as in Eq. (12) then becomes

$$F=\int\left\{\tfrac{1}{2}\kappa\left(\nabla^2 h\right)^2+\tfrac{1}{2}k\left[\left(\rho^+ +d\nabla^2 h+\varepsilon\right)^2+\left(\rho^- -d\nabla^2 h\right)^2\right]\right\}dxdy. \quad (15)$$

Carrying out a derivation equivalent to Eq. (14) and considering the fact that $\eta q_0 \ll b_f$ and $\mu q_0^2 \ll b_f$ for the lipid bilayer, the relaxation dynamics for the chemically modified bilayer can be written as

$$\frac{\partial}{\partial t}\begin{pmatrix} h \\ \rho+\varepsilon \end{pmatrix} = -\begin{pmatrix} \tilde{\kappa}{q_0}^3/4\eta & -q_0 kd/2\eta \\ -kd{q_0}^4/2b_f & k{q_0}^2/2b_f \end{pmatrix} \cdot \begin{pmatrix} h \\ \rho+\varepsilon \end{pmatrix}. \quad (16)$$

The eigenvalues of this modified dynamical matrix are

$$\gamma_{1,2} = \frac{1}{2}\left[\frac{\tilde{\kappa}{q_0}^3}{4\eta} + \frac{k{q_0}^2}{2b_f} \pm \sqrt{\left(\frac{\tilde{\kappa}{q_0}^3}{4\eta} - \frac{k{q_0}^2}{2b_f} \right)^2 + \frac{k^2 d^2 {q_0}^5}{\eta b_f}} \right]. \quad (17)$$

We have $h(t) = Pe^{-\gamma_1 t} + Qe^{-\gamma_2 t}$, with P and Q determined by the initial conditions: $h(t = 0) = 0$ and $\rho(t = 0) = -\varepsilon/2$. This leads to:

$$h(0) = P + Q = 0$$

$$h'(0) = -\gamma_1 P - \gamma_2 Q = \frac{q_0 kd\varepsilon}{4\eta},$$

giving

$$P = -Q = \frac{q_0 kd\varepsilon}{4\eta(\gamma_2 - \gamma_1)}.$$

Finally,

$$h(t) = \frac{q_0 kd\varepsilon}{4\eta(\gamma_2 - \gamma_1)}\left(e^{-\gamma_1 t} - e^{-\gamma_2 t} \right). \quad (18)$$

From Eq. (18) we see that the membrane undulation converges to zero at infinite time, thus indicating stability of the bilayer. At $t = \ln(\gamma_1/\gamma_2)/(\gamma_1 - \gamma_2)$, $h(t)$ achieves its maximum:

$$h_{\max} = \frac{q_0 kd\varepsilon}{4\eta\gamma_1}\left(\frac{\gamma_2}{\gamma_1} \right)^{\gamma_2/(\gamma_1 - \gamma_2)}. \quad (19)$$

For a few percent variation of the effective headgroup area ($\varepsilon \sim 0.01$), h_{max} can easily achieve a macroscopic value (~1 μm). By measuring the shape undulation of the chemically modified vesicle, the inter-leaflet friction coefficient was fitted as 2×10^9 J ·s ·m^{-4} [8], in good agreement with the most recently measured value mentioned above. More realistic and complicated models were also discussed by Bitbol and Fournier: spontaneous curvature of the membrane was accounted for and was allowed to be modified by chemicals [5,64]; both the membrane binding kinetics and the effect of inhomogeneous concentration of chemicals were examined [65].

3. Membrane tension

3.1. Entropic tension as result of geometrically constraining membrane fluctuations

As we discussed above, membranes undergo thermally excited shape fluctuations to increase their configurational entropy [2]. In reality, instead of being a free-floating bilayer, biological membranes are usually constrained by the shape of the cell and the dynamic coupling with the cytoskeleton [19,24,54,66,67]. The geometrical constraints imposed by the membrane shape, or any external restrictions, will reduce the configurational entropy and create a lateral tension in the membrane [50,68]. Taking these contributions into account, the free energy as in Eq. (2) should then be written as,

$$F=\int \tfrac{1}{2}\left\{\kappa\left(\nabla^2 h\right)^2+\sigma|\nabla h|^2+\Omega h^2\right\} dxdy \quad (20)$$

where σ is membrane tension and $\Omega = d^2V/dz^2|_{z=0}$ again, represents the contribution from the harmonic interaction potential. Accordingly, the fluctuation spectrum as determined from the equipartition theorem is modified to yield [20,69],

$$\left\langle |h(q)|^2 \right\rangle = \frac{k_B T}{A(\kappa q^4+\sigma q^2+\Omega)}. \quad (21)$$

Macroscopic observation of projected surface area as a function of membrane tension allows determining the compressibility of membranes. The decrease of effective or projected membrane area relative to the real membrane surface area (ΔA) due to the undulations can be calculated from the fluctuation amplitude [50],

$$\Delta A = -\frac{1}{2}\int_A |\nabla h|^2 dA \quad (22)$$

or more conveniently, in Fourier space

$$\Delta A(q) = -\frac{A}{2} q^2 |h(q)|^2. \quad (22')$$

Eqs. (21) and (22′) lead to,

$$\Delta A = \sum_q \Delta A(q) = \sum_q \frac{-k_B T q^2}{2(\kappa q^4+\sigma q^2+\Omega)}. \quad (23)$$

Replacing the sum by an integral,

$$\sum_q \rightarrow \frac{A}{(2\pi)^2}\int 2\pi q t q \quad (24)$$

and considering the lower and upper limit for the integration as defined by $\pi/A^{0.5}$ ($A \sim L^2$) and π/a_0, the total decrease of projected area can be calculated from Eqs. (23) and (24),

$$\frac{\Delta A}{A} = \frac{-k_B T}{8\pi\kappa} \int_{\pi/A^{0.5}}^{\pi/a_0} \frac{q^2 dq^2}{q^4 + (\sigma/\kappa) q^2 + \Omega/\kappa} = \frac{k_B T}{8\pi\kappa \sqrt{(\sigma/\kappa)^2 - 4(\Omega/\kappa)}} \left[x_1 \ln \frac{\pi^2/A - x_1}{\pi^2 {a_0}^2 - x_1} - x_2 \ln \frac{\pi^2/A - x_2}{\pi^2/{a_0}^2 - x_2} \right] \quad (25)$$

with, $x_{1,2} = \frac{-\sigma/\kappa \pm \sqrt{(\sigma/\kappa)^2 - 4(\Omega/\kappa)}}{2}$.

In the limit of $\sigma \gg \kappa\Omega$, $x_1 = 0$ and $x_2 = -\sigma/\kappa$. Eq. (25) then simplifies to,

$$\frac{\Delta A}{A} = \frac{k_B T}{8\pi\kappa} \ln \frac{\pi^2/A + \sigma/\kappa}{\pi^2/{a_0}^2 + \sigma/\kappa}. \quad (25')$$

Thus, a certain amount of area is hidden in the roughness of membrane undulations. At zero tension, the amount of hidden area is $|\Delta A/A| = k_B T/8\pi\kappa \times \ln (A/{a_0}^2)$; increasing membrane tension will serve to flatten out undulations and increase projected area. If we define ΔA_{exp} as the change of membrane area relative to the initial membrane state with tension σ_0, then Eq. (25′) changes into the more commonly used format [70],

$$\frac{\Delta A_{\exp}}{A} = \frac{k_B T}{8\pi\kappa} \ln \frac{1/A\sigma/\pi^2\kappa}{1/A\sigma_0/\pi^2\kappa}. \quad (25'')$$

When a stretching force is applied to the bilayer (experimentally this is usually done by aspirating a vesicle with hydrostatic pressure [68,71] or by expanding the substrate of a supported lipid bilayer [67,72]), entropic tension adds to the normal elastic stretch response of a fluid membrane [50]. Thus, the total area change (ΔA_t) as one increases membrane tension (compared to the initial $\sigma = \sigma_0$ membrane) can be written as

$$\frac{\Delta A_t}{A} = \frac{k_B T}{8\pi\kappa} \ln \frac{1 + A\sigma/\pi^2\kappa}{1 + A\sigma_0/\pi^2\kappa} + \frac{\sigma - \sigma_0}{K} \quad (26)$$

where K is the elastic modulus of membrane stretching.

Accordingly, two different regimes of membrane tension response to stretching of the projected area can be observed: In the low-tension regime, Eq. (26) is dominated by the entropic term and membrane area will increase logarithmically with tension. In the high-tension regime, the enthalpic or elastic stretching term becomes important, leading to a linear relation between area and tension. By fitting experimental data in the two regimes, bending and elastic stretching moduli can be extracted respectively, and the crossover tension for the two regimes is found to be around 0.5 mN/m [68]. This two-regime behavior

is also verified by CG simulations [73], from which one can obtain a more detailed description of the structural rearrangements of bilayers under tension.

For simplicity, we used a plane-wave approximation in treating fluctuation modes. For vesicles, it is more appropriate to expand the membrane with respect to a spherical shape [74]. However, the resulting physical relations are very similar. Regarding Eq. (26), for example, in the quasi-spherical approach, we only need to change the pre-factor for membrane tension from π^2 to 24π [68]. For a discussion of the entropic tension of non-spherical shapes, and more precise evaluation of the tension induced by constraining membrane fluctuations, see Ref. [75].

In deriving Eq. (25), the conservation of total membrane area sets a constraint that relates entropic tension to the hidden membrane area. During membrane fusion, however, lipids will be added into the bilayer and total membrane area will increase. Studies have shown both theoretically [76], and by experiments [77], that during fusion of oppositely charged vesicles, membrane tension will become negative and local instabilities of the vesicle can occur. Conversely, increasing membrane tension was found by mesoscopic simulations to facilitate the fusion of vesicles into membrane bilayers [78]. Another example of tension regulation of the membrane area was demonstrated by reversibly straining a lipid bilayer that was coupled to an elastic PDMS sheet [67,72]. By stretching the elastic support, the bilayer expands laterally by fusing adhered lipid vesicles which compensates for the membrane tension induced by the lateral strain. Upon compression, spherical or tubular protrusions are found to nucleate and subsequently grow out of the membrane [72]. The formation of tubules under compression indicates the existence of a critical (negative) membrane tension, beyond which the planar bilayer is destabilized and expels lipid tubes to relax its area in the plane [67]. The membrane tubes, stabilized by a negative pressure imbalance between two sides of the bilayer, transform its shape dynamically when the liquid volume enclosed between the bilayer and PDMS sheet is changed. Interestingly, the tubules will thin out, collapse, and detach after a rapid decrease in liquid volume [72].

3.2. Biological significance of membrane tension

The role of membrane tension in regulating dynamic cellular behaviors is gaining attention in recent years, with studies ranging from cell shape and motility, exo- and endocytosis, to intracellular signaling and gene expression [53,79–88]. Cells are known to maintain their unique membrane tensions which usually arise from two sources: hydrostatic pressure across the lipid bilayer and cytoskeleton-membrane adhesion [53]. The latter contribution is postulated to play the primary role, considering the large surface area-to-volume ratio of most mammalian cells [52]. However, separating the relative magnitude of each source is difficult since they are not independent from each other [83]. In order for the cells to maintain a relatively stable membrane tension, sudden tension changes need to be buffered by depleting/restoring membrane reservoirs [81,83]. Membrane reservoirs can store 20%–40% of the plasma membrane area and usually exist in the form of membrane folds, caveolae and blebs [80,83].

The dynamic membrane shape transition required for cell migration is determined by the elastic free energy of the membrane, in which tension plays a major role. Membrane tension

is also closely involved in the regulation of membrane trafficking processes since the addition or removal of lipids during vesicle fusion or fission directly alters the magnitude of stress in the membrane. Generally speaking, increasing membrane tension will slow down the rate of cell motility [88,89], activate exocytosis [82], and inhibit endocytosis [90]. Particularly, during the membrane invagination stage of clathrin-mediated endocytosis (CME), vesicles can easily form when membrane tension is low, however, extra force from actin polymerization is required if the cellular plasma membrane is under high tension [91].

4. Membrane shape instability

4.1. Spontaneous tubulation and membrane curvature instability

As discussed above, negative membrane tension accomplished by physically compressing or adding lipids into the membrane could cause a planar membrane to become unstable, leading to the formation of non-planar shapes, including membrane tubules [67,77]. Spontaneous tubule formation can also be triggered chemically by the binding of polymers [92,93] or even the addition of a simple basic pH solution to giant vesicles, as mentioned above [8]. More importantly, membrane tubules play important biological roles and can be induced by membrane curvature sensing and generating proteins [38]. Some peptides are also known to induce protrusions from supported lipid bilayers [94]. Real-time tubulation of giant vesicles has recently been observed for F-BAR domain proteins [95]. However, unlike the dynamics of membrane fluctuations, the rate and mechanism of membrane tube formation have not been well described.

There are numerous phenomena involving membrane shape instabilities. Apart from the above-mentioned spontaneous membrane tubulation, externally applied perturbations such as by means of optical tweezers or the anchoring of polymers/nanoparticles can induce a pearling instability [96–99]. Vesicles can also undergo shape transitions induced by temperature change or by the coupling between local membrane composition and curvature [19,100–103]. Among these phenomena, the ones induced by macromolecule- (in particular protein-) binding to membranes are especially interesting due to their biological significance.

Several models have been proposed to explain membrane shape instabilities [15,34,93,104,105]. The model directly applicable to curvature-inducing proteins considers the coupling between membrane curvature and protein density [34,99]. When a planar membrane becomes unstable, the effective bending rigidity of the membrane will become zero and shape fluctuations of the membrane will increase with time until reaching macroscopic levels [34]. Here, we will once again mainly focus on membranes with a near-planar geometry, so that membrane fluctuations can be easily represented by planar waves. For membrane shape transitions between nontrivial configurations, extensive discussions can be found in the following contributions [19,100,106,107].

Proteins with a normalized local density φ (equivalent to fractional protein coverage, ranging from 0 to 1) can diffuse in the membrane with a diffusion coefficient D. The interaction between proteins can be described by the Ginsburg–Landau free energy [34,48,108],

$$F_{protein}=\int\left\{\frac{1}{2}a\phi^2+\frac{1}{2}b|\nabla\phi|^2\right\}dxdy \quad (27)$$

where 'a' is the inverse osmotic compressibility which is dependent on protein density [109], 'b' is normally a constant and can be expressed (in a simple lattice model) as, '$\lambda/\beta\cdot k_BT$' where β is the excluded area of the protein and λ represents an effective 'interaction area' for molecular interactions a protein density gradient [110]. The first term describes the free energy density for a homogeneous system while the second term represents the energy cost of inhomogeneous protein distribution.

If the protein has an intrinsic curvature, as most curvature sensing and generating proteins do [38], the elastic energy of the bilayer with the contribution from membrane tension will be written as:

$$F_{elastic}=\int\left\{\frac{1}{2}\kappa\left[\left(\nabla^2h\right)-C_0\phi\right]^2+\frac{1}{2}\sigma|\nabla h|^2\right\}dxdy \quad (28)$$

where C_0 describes the spontaneous curvature of the membrane induced by protein binding.

For simplicity, the coupling between protein and membrane is assumed to be isotropic and the contributions from membrane inter-leaflet friction and the interaction potential $V(z)$ are not considered in the following dynamic analysis. We will briefly discuss the modification of membrane instability criteria in the presence of a harmonic interaction potential at the end of this section. For inclusions anisotropically coupled to membrane curvature, the Gaussian curvature of the membrane will be affected in addition to the mean curvature [111,112].

It can be easily seen from Eq. (28) that the presence of spontaneous curvature leads to an effective coupling between protein density and local membrane shape, with the coupling strength described by κC_0.

$$F_{couple}=-\int\kappa C_0\phi\nabla^2h\,dxdy. \quad (29)$$

Thus the total energy of the membrane and protein can be written as,

$$F=\int\left\{\frac{1}{2}\kappa\left(\nabla^2h\right)^2+\frac{1}{2}\sigma|\nabla h|^2-\kappa C_0\phi\nabla^2h+\frac{1}{2}a_{eff}\phi^2+\frac{1}{2}b|\nabla\phi|^2\right\}dxdy \quad (30)$$

here, $a_{eff}=a+\kappa C_0^2$ is the effective inverse osmotic compressibility after accounting for the spontaneous curvature of a membrane patch covered by a protein molecule. Both a_{eff} and b are assumed to be positive to exclude the situations of spontaneous demixing of proteins [34].

The dynamics of the bulk liquid is still determined by the Navier–Stokes equation (Eqs. (5) and (6)) and the corresponding force balance equations at the membrane–bulk liquid interface (Eq. (7)). The restoring force of the membrane includes the contributions from membrane tension and protein distribution:

$$\begin{aligned} T_{xz}|_{z=0} &= \eta\left(\frac{\partial v_x}{\partial z}+\frac{\partial v_z}{\partial x}\right)\Big|_{z=0}=0 \\ T_{zz}|_{z=0}=P_z=-\frac{\delta F}{\delta h} &\iff \left(2\eta\frac{\partial v_z}{\partial z}-p\right)\Big|_{z=0}=-\kappa q_0{}^4 h-\sigma q_0{}^2 h-\kappa C_0 q_0{}^2 c. \end{aligned} \quad (7')$$

Here, $c(x,y) \equiv \varphi(x,y) - \varphi_{avg}$ is the deviation of local protein density from its average value φ_{avg}, and it is assumed to follow $c = c_0 e^{iq_0 x + iwt}$.

Motions of the membrane and of the proteins on the membrane are described by

$$\begin{aligned} \frac{\partial h}{\partial t} &= v_z|_{z=0}=(C_3+C_4)e^{iq_0 x+iwt} \\ \frac{\partial c}{\partial t}=\nabla\cdot\vec{j} &= \frac{D}{a_{eff}}\nabla^2\left(\frac{\delta F}{\delta c}\right)=-Dq_0{}^2 c-\frac{b}{a_{eff}}Dq_0{}^4 c-\frac{\kappa C_0 D}{a_{eff}}q_0{}^4 h. \end{aligned} \quad (31)$$

The first equation is identical to Eq. (8) with C_3 and C_4 representing the constants determined by the new set of boundary conditions in Eq. (7′). The second equation describes the diffusion of proteins on the membrane. Here, protein binding from the bulk liquid is ignored since protein/membrane binding is usually diffusion-controlled and the diffusion of protein in the bulk solution is typically much faster than on the lipid membrane. If protein molecules binding to and unbinding from the membrane are considered, the time dependence of the local protein density will be modified to [48],

$$\frac{\partial c}{\partial t}=-\left(Dq_0{}^2+\frac{L\xi}{\tau(1+L\xi)}\right)\left[\left(1+\frac{b}{a_{eff}}q_0{}^2\right)c+\frac{\kappa C_0 q_0{}^2}{a_{eff}}h\right] \quad (31')$$

where $L=\sqrt{q_0{}^2+iw/D_b}$, D_b and ξ are the protein's diffusion coefficient and characteristic diffusion length in the bulk, respectively, and t is the residence time of the protein on the membrane. The presence of bulk diffusion will affect the fluctuation spectrum. For example, an oscillatory damping mode emerges at large q_0, but the curvature instability criteria will not be changed as discussed in Ref. [48].

In Eq. (31), C_3 and C_4 can be determined from Eq. (7′) and the resulting equation of motion for the membrane is:

$$\frac{\partial}{\partial t}\begin{pmatrix} h \\ c \end{pmatrix}=-\begin{pmatrix} \kappa q_0{}^4 m+\sigma q_0{}^2 m & \kappa C_0 q_0{}^2 m \\ \frac{\kappa C_0 D q_0{}^4}{a_{eff}} & \left(Dq_0{}^2+\frac{bDq_0{}^4}{a_{eff}}\right) \end{pmatrix}\cdot\begin{pmatrix} h \\ c \end{pmatrix}. \quad (32)$$

Here, m is independent of h and c

$$m=\frac{iw\rho q_0}{4q_0{}^3\eta^2(q_0-l)+4iw\rho q_0{}^2\eta-w^2\rho^2}. \quad (33)$$

Using $h = h_0 e^{iq_0 x+iwt}$ and $c = c_0 e^{iq_0 x+iwt}$, Eq. (32) gives the dispersion relation of the system:

$$(S_0-1)^2-\sqrt{1-2S_0}+y_t+\frac{\chi}{S_0\zeta-bq_0{}^2/a_{eff}-1}=0 \quad (34)$$

with unitless variables defined as

$$S_0=\frac{-iw\rho}{2\eta q_0{}^2}, y_t=\frac{(\kappa q^2+\sigma)\,\rho}{4\eta^2 q_0}, \chi=\frac{\rho\kappa^2 C_0{}^2 q_0}{4\eta^2 a_{eff}}, \zeta=\frac{2\eta}{\rho D}.$$

When there is no coupling between protein density and membrane curvature ($C_0 = 0$), Eq. (34) reduces to Eq. (9′).

In the slow mode limit ($S_0 \ll 1$), since $1/\zeta \sim 10^{-8} \ll 1$, and if we can also assume $bq_0^2/a_{eff}\zeta \ll 1$ as in [34], the dispersion relation approximates to:

$$S_0{}^2-S_0\left(y_t+\frac{bq_0{}^2}{a_{eff}\zeta}+\frac{1}{\zeta}\right)+y_t\left(\frac{bq_0{}^2}{a_{eff}\zeta}+\frac{1}{\zeta}\right)-\frac{\chi}{\zeta}=0. \quad (35)$$

The fluctuation modes as the roots of the dispersion relation are:

$$iw_{\pm}=-\left[\frac{\kappa q_0{}^3+\sigma q_0}{4\eta}+\frac{Dq_0{}^2}{2}+\frac{bDq_0{}^4}{2a_{eff}}\pm\sqrt{\left(\frac{\kappa q_0{}^3+\sigma q_0}{4\eta}-\frac{Dq_0{}^2}{2}-\frac{bDq_0{}^4}{2a_{eff}}\right)^2+\frac{\kappa^2 C_0{}^2 Dq_0{}^5}{2a_{eff}\eta}}\right]. \quad (36)$$

Here, iw is always real, indicating that the mode remains non-propagating [34]. Fig. 4 shows iw as a function of q_0 for both zero and non-zero tension situations.

While the iw_+ branch is negative for all values of q_0, iw_- can become positive in certain situations for $q^*_- < q_0 < q^*_+$ (in the case of zero tension, $q^*_- = 0$), indicating the possibility of unstable modes. q^* can be easily determined by equating iw_- to zero:

$$q*_{\pm}=\sqrt{\frac{-\left(\kappa a_{eff}+b\sigma-\kappa^2 C_0{}^2\right)\pm\sqrt{\left(\kappa a_{eff}+b\sigma-\kappa^2 C_0{}^2\right)^2-4a_{eff}b\sigma\kappa}}{2b\kappa}}. \quad (37)$$

Thus, the criterion for the existence of unstable fluctuation modes is equivalent to the existence of real values for q^* satisfying Eq. (37), which is:

$$\kappa^2 C_0{}^2-a_{eff}\kappa-b\sigma \geq \sqrt{4a_{eff}b\sigma\kappa} \quad (38)$$

or

$$\sqrt{a_{eff}\kappa}+\sqrt{b\sigma} \leq \kappa|C_0|. \quad (38')$$

If $bq_0^2/a_{eff}\zeta \ll 1$ does not hold, Eq. (35) becomes,

$$\left(1+\frac{3bq_0{}^2}{2a_{eff}\zeta}\right)S_0{}^2-S_0\left(y+\frac{bq_0{}^2}{a_{eff}\zeta}+\frac{1}{\zeta}\right)+y\left(\frac{bq_0{}^2}{a_{eff}\zeta}+\frac{1}{\zeta}\right)-\frac{\chi}{\zeta}=0. \quad (35')$$

However, the expression for q^* is not altered, because q^* was determined by equating the constant term (0th order term in S_0) in Eq. (35) to zero. Thus, the curvature instability criterion shown in Eq. (38) is the same irrespective of the magnitude of $bq_0^2/a_{eff}\zeta$.

The instability criterion does not contain any information about the dynamics of the system (that is, η or ρ for the hydrodynamics of the bulk liquid and D for the diffusion of proteins on membrane), meaning that we should be able to obtain Eq. (38) directly from the free energy of the membrane and protein. This will be shown in the following.

From Eq. (30), the free energy density can be written as,

$$\begin{aligned} f\sim&=\tfrac{1}{2}\kappa\left(\nabla^2 h\right)^2+\tfrac{1}{2}\sigma|\nabla h|^2-\kappa C_0\phi\nabla^2 h+\tfrac{1}{2}a_{\mathrm{eff}}\phi^2+\tfrac{1}{2}b|\nabla\phi|^2 \\ &=\tfrac{1}{2}\kappa q_0{}^4h^2+\tfrac{1}{2}\sigma q_0{}^2|h|^2+\kappa C_0 q_0{}^2\phi\mathrm{h}+\tfrac{1}{2}a_{\mathrm{eff}}\phi^2+\tfrac{1}{2}bq_0{}^2|\phi-\phi_{\mathrm{avg}}|^2. \end{aligned} \quad (39)$$

The breakdown of local thermodynamic stability is described by the spinodal equation [113],

$$\frac{\partial^2\tilde{f}}{\partial h^2}\frac{\partial^2\tilde{f}}{\partial\phi^2}-\left(\frac{\partial^2\tilde{f}}{\partial h\partial\phi}\right)^2=\left(\kappa q_0{}^4+\sigma q_0{}^2\right)\left(a_{eff}+bq_0{}^2\right)-\kappa^2C_0{}^2q_0{}^4=0 \quad (40)$$

which is equivalent to Eq. (37) and the resulting instability criterion is the same as Eq. (38) [48].

In the presence of the interaction potential $V(z)$, an additional term $\Omega h^2/2$ should be added to Eq. (39), modifying the spinodal equation to,

$$\left(\kappa q_0{}^4+\sigma q_0{}^2+\Omega\right)\left(a_{eff}+bq_0{}^2\right)-\kappa^2C_0{}^2q_0{}^4=0. \quad (40')$$

Therefore, the instability criterion becomes equivalent to the existence of a real and positive q_0, which satisfies Eq. (40′). Analyzing this third order (in q_0^2) equation gives the instability criterion in the presence of the harmonic interaction potential,

$$\kappa^2C_0{}^2-a_{eff}\kappa-b\sigma>\sqrt{3b\kappa\left(a_{eff}\sigma+b\Omega\right)} \quad (38''.1)$$

and

$$\left[2\sqrt{\left(\kappa^2{C_0}^2-a_{eff}\kappa-b\sigma\right)^2-3\left(a_{eff}\kappa b\sigma+b^2\kappa\Omega\right)}-\left(\kappa^2{C_0}^2-a_{eff}\kappa-b\sigma\right)\right]\cdot$$
$$\left[\sqrt{\left(\kappa^2{C_0}^2-a_{eff}\kappa-b\sigma\right)^2-3\left(a_{eff}\kappa b\sigma+b^2\kappa\Omega\right)}+\left(\kappa^2{C_0}^2-a_{eff}\kappa-b\sigma\right)\right]^2\geq 27ab^2\kappa^2\Omega. \quad (38'')$$

If $\Omega = 0$, these two equations reduce to Eq. (38). It can be seen from the instability criteria that (positive) σ and Ω serve to stabilize the membrane.

From equilibrium analysis, the height fluctuation can also be easily determined from the equipartition theorem,

$$<|h(q)|^2>=\frac{k_BT\left(a_{eff}+bq^2\right)}{A\left[\left(\kappa q^4+\sigma q^2+\Omega\right)\left(a_{eff}+bq^2\right)-\kappa^2{C_0}^2q^4\right]}. \quad (41)$$

Thus, the stability of a planar membrane is only determined by the system's free energy. However, dynamic analysis is required to understand the detailed behaviors of the membrane while crossing into the unstable regime. For example, the fluctuation modes in Eq. (36) which correspond to the rate of macroscopic membrane shape change can only be given by solving the dynamic equations. The dynamic analyses of membrane shape instability in the presence of cytoskeleton–membrane interactions are discussed in Refs [87,114].

4.2. Membrane shapes after planar geometry becomes unstable

A remaining question is what kinds of shapes the membrane will transform into after the planar geometry becomes unstable, for example due to proteins binding to and coupling with curvature of the membrane. Experiments indicate the formation of membrane tubules [8,92,95,115] or microvesicles [116,117] when a flat membrane experiences a curvature instability. Phenomena such as the formation of membrane protrusions during RBC crenation [34,48] and the curling of ruptured RBC membranes [118] could also be the results of curvature instabilities. Once the instability threshold is reached, nonlinear effects become important (such as, membrane shape can no longer be accurately described by the small slope approximation as in Eq. (2)) and accurate shape transitions of the membrane can only be evaluated numerically. A simplified simulation of a one-dimensional membrane indicated the development of membrane fingers and buds (depending on the strength of the curvature coupling) with a tendency toward vesicle emission [48].

Another way to understand the phase diagrams of new membrane shapes is through a mean-field treatment of the Ginsburg–Landau free energy. In this approach, mean field energies of different undulated phases (represented by trial functions with undulation wavelengths determined by the coupling strength) are compared with the planar homogeneous phase to figure out the lowest energy configuration [119]. In-plane meso-structures such as stripe phase and hexagonal phase will form when the coupling strength is strong. In the case of anisotropic coupling, membrane phases of both positive and negative curvature can be induced [120]. Similar methods can also be applied to study buckling phenomena of lipid

monolayers [121,122] or polymer thin films which, unlike fluid lipid layers, have a non-zero in-plane shear elasticity [123].

5. Peripheral proteins on membranes

5.1. Membrane-mediated protein interactions

Apart from the lipid bilayer structure, proteins are major components of biological membranes. Thus, it is important to understand variations of membrane shapes and fluctuation spectra in the presence of protein inclusions. Membrane inclusions can perturb the bilayer structure and impose restrictions on thermal fluctuations; both effects will lead to membrane-mediated modifications of the interaction between inclusions [120,124–127]. The disturbance-induced attraction is short-ranged, fading away exponentially with a characteristic length $l_0 \equiv (\kappa/\sigma)^{1/2}$ [124,126]. The fluctuation-mediated interaction falls off as $1/R^4$ for a distance $R \ll l_0$ [126,127]. For $R \gg l_0$, the distance dependence becomes $1/R^8$ [126]. The latter force, which exists as long as there is a difference between membrane and inclusion rigidity, will dominate at a length scale large comparable to the dimension of the inclusion. More comprehensive descriptions of the fluctuation-induced force between inclusions of arbitrary shapes embedded in membranes under tension can be found in Refs. [126,128].

Energetically speaking, the perturbation of the fluctuation spectrum will contribute to the free energy associated with protein or peptide insertion into the membrane. Thus, the larger fluctuations of low-tension membranes will make it harder for inclusions to incorporate into the lipid bilayer compared with the corresponding high-tension situation [120]. The diffusion of these fluctuation-suppressing particles on membranes is also expected to be slowed when membrane tension is increased [129].

The influence of proteins on fluctuation spectra and thus membrane tension has been relatively well studied for active membranes [130,131]. The presence of active protein pumps adds a non-equilibrium noise source to the dynamic equations. This will lead to an amplification of membrane fluctuations, equivalent to an increase of effective temperature or decrease in effective bending rigidity in Eq. (26) [130]. Additionally, membranes will become thinner under tension, which affects the hydrophobic mismatch interaction between membrane inclusions [73]. Thus, by properly controlling membrane tension, one may control the amount, and the distribution, of proteins on the membrane.

Coarse-grained simulations revealed that proteins adsorbed on lipid bilayers can experience attractive interactions purely as a result of induced-membrane curvature [6], similar to what was observed for the much larger membrane-bound colloidal particles [132]. For proteins with an intrinsic curvature or anisotropic shape, this curvature-mediated attraction can lead to spontaneous aggregation and formation of highly ordered protein structure on the membrane [6,133–135]. Additionally, the interactions between membrane inclusions depend on factors such as charge and hydrophobicity of the inclusions, and their hydrophobic mismatch or orientation relative to the membrane [6,124,136,137].

5.2. Protein assemblies on membranes and protein-induced membrane shape transitions

As discussed above, there are many different types of forces leading to protein aggregation on membranes. Formation of aggregates may significantly change the physical properties and membrane interaction behaviors of protein [136]. Thus, the aim to understand membrane binding and subsequent two-dimensional assembly of peripheral proteins has become an active area of research. Biologically, this is important for understanding protein-mediated cellular membrane phenomena such as exo- and endocytosis, protein sorting, and biogenesis of organelles such as the endoplasmic reticulum and the Golgi apparatus [6,137]. Clathrin-mediated endocytosis as one of such processes has become better understood in recent years [7,138]. During CME, the engulfing of cargo through membrane invagination and subsequent vesicle formation requires coordinated action of more than 30 proteins, ranging from clathrin, adaptor proteins, and epsin, to BAR domain proteins and dynamin [39,139–142]. Thus, topics such as membrane binding kinetics, assembly and cooperativity between these proteins on membranes are of essential biological importance.

The structure of many membrane binding interfaces of most endocytic proteins have been well characterized by crystallography studies [7]. For proteins with a high intrinsic curvature such as BAR domain proteins, ordered protein lattices were directly observed on highly curved membrane tubules through cryo-electron microscopy [143,144]. However, little attention has been paid to these proteins' dynamic behaviors on membranes with low curvature, which is critical for revealing the curvature initiation process during endocytosis. Thus, there exists a clear gap between our understandings of these proteins' intrinsic molecular properties and their final configurations on highly curved endocytic structures. Studies of protein–membrane interaction dynamics will serve to link this gap.

Kinetic membrane binding studies of endocytic proteins have been initiated a few years ago [145,146]. More recently, endophilin, which is an N-BAR domain protein, was found to be able to oligomerize on relatively flat membranes both experimentally [147] and through CG simulations[148,149]. The presence of an oligomerization step in the protein–membrane interaction mechanism highlights the role of protein density in this dynamic process. For example, in the study of membrane interaction kinetics of endophilin, the protein density dependence of the observed dissociation rate turns out to be the key evidence to confirm the presence of protein oligomers on flat membranes [147]. In experiments probing membrane curvature sorting of amphiphysin, another N-BAR domain protein, protein density was argued to determine the mechanism by which amphiphysin can sense membrane curvature [150]. CG simulations have also shown a critical particle number required for driving the formation of small vesicle buds [151], further supporting the idea that protein density is a regulator of two-dimensional protein assembly on the membrane.

From simulation studies, it was concluded that the aggregation of particles precedes membrane vesiculation and tubulation [6,134,152], and a sufficiently high density of particles is needed to influence membrane topography [151,153]. Experimentally, protein concentrations leading to near saturation of proteins on the membrane surface were used when studying the formation of protein lattices on membrane tubules [143,144]. Taking these together, it is tempting to speculate that, at least for BAR domain proteins, the oligomerization of proteins on the membrane acts as a precursor for the generation of highly

curved membrane structures and the overall dynamic process is controlled by protein density on the membrane. This has been suggested to explain experimental observations using simpler peptides, where membrane-bound peptides were found to undergo an in-plane segregation before inducing membrane tubules at higher peptide density [94].

6. Conclusion and perspectives

The purpose of this review is to reemphasize the dynamic nature of cellular membranes. There are numerous fascinating phenomena associated with the thermal fluctuations of the lipid bilayer. Some of them, e.g. dissipation modes of small fluctuations, fluctuation-induced membrane tension, and membrane-mediated force between membrane inclusions, were reviewed in the foregoing discussions. On the way to understanding the dynamic behavior of cellular membranes, currently the most intriguing challenge is to understand the influence of membrane proteins on the dynamics of lipid bilayers. As a first step toward resolving the open questions, we reviewed the linear theory regarding the modification of membrane fluctuation spectra in the presence of diffusive proteins. There, instability of planar membranes arises as a result of the coupling between protein density and membrane shape. The recent progress in understanding the assembly of curvature inducing proteins on membranes was also discussed. Protein density on the membrane is proposed as a key factor in regulating the behavior of proteins on the membrane as well as the effect of proteins on membrane geometry.

We suggest the following topics for further attention in future research:

1. Fully characterizing the dynamics of protein-induced membrane shape instabilities will be a key to our understanding of the behaviors of biological membranes. Experimentally, we need to identify and characterize the factors that control the instability process.
2. It is also important to understand the physical properties of protein-decorated membranes in more detail, such as the fluctuation spectra and bending rigidities of protein-covered membranes. The possibility of tubular/planar membrane shape coexistence will make this task nontrivial. Simulation studies can provide additional guidance for designing experiments in this part. Towards accomplishing this goal, the flexibility of a protein-coated membrane tube was recently calculated [134].
3. Considering the various types of proteins involved in biological processes, another important issue is to understand the cooperativity between different types of proteins as well as proteins of the same species. Cooperativity of membrane binding between BAR domain proteins and dynamin has been examined recently [154]. However, a theoretical description of the cooperative kinetics is still missing. For example, studies regarding the cooperativity between the same kind of proteins during membrane binding are still mostly at a theoretical level [155]. Interestingly, it has been suggested by theoretical studies that different protein species may segregate on the membrane according to their intrinsic curvature [134,135], similar to what has been observed in in vivo experiments [156].

4. It is well known that the charge [147,157] and packing defects [158,159] of lipid bilayers can greatly influence protein/membrane binding kinetics and affinity. It is likely that these factors can also regulate the protein behaviors on the membrane such as their lateral diffusion and aggregation ability as well as their coupling strength with membrane curvature.

5. For simulation studies of membrane shape transitions and protein–membrane interactions, we suggest that membrane tension should be considered with a high priority. This is because, as discussed above, membrane tension may significantly influence the binding and assembly of proteins on the membrane. Additionally, membrane tension factors into the instability criterion of the planar membrane geometry and determines the dynamics of membrane shape transitions.

Acknowledgments

We thank Drs. T. C. Lubensky and K. J. Stebe for enlightening discussions. This contribution was funded by NSF Grant CBET 1053857 and MRSEC Grant DMR 11-20901, and NIH Grant R01 GM097552.

References

1. Bonifacino JS, Glick BS. The mechanisms of vesicle budding and fusion. Cell. 2004; 116:153–66. [PubMed: 14744428]
2. Lipowsky R. The conformation of membranes. Nature. 1991; 349:475–81. [PubMed: 1992351]
3. McMahon HT, Gallop JL. Membrane curvature and mechanisms of dynamic cell membrane remodelling. Nature. 2005; 438:590–6. [PubMed: 16319878]
4. Shibata Y, Hu JJ, Kozlov MM, Rapoport TA. Mechanisms shaping the membranes of cellular organelles. Annu Rev Cell Dev Biol. 2009; 25:329–54. [PubMed: 19575675]
5. Bitbol AF, Fournier JB, Angelova MI, Puff N. Dynamical membrane curvature instability controlled by intermonolayer friction. J Phys Condens Matter. 2011:23.
6. Reynwar BJ, Illya G, Harmandaris VA, Muller MM, Kremer K, Deserno M. Aggregation and vesiculation of membrane proteins by curvature-mediated interactions. Nature. 2007; 447:461–4. [PubMed: 17522680]
7. McMahon HT, Boucrot E. Molecular mechanism and physiological functions of clathrin-mediated endocytosis. Nat Rev Mol Cell Biol. 2011; 12:517–33. [PubMed: 21779028]
8. Fournier JB, Khalifat N, Puff N, Angelova MI. Chemically triggered ejection of membrane tubules controlled by intermonolayer friction. Phys Rev Lett. 2009:102.
9. Sciaky N, Presley J, Smith C, Zaal KJM, Cole N, Moreira JE, et al. Golgi tubule traffic and the effects of Brefeldin A visualized in living cells. J Cell Biol. 1997; 139:1137–55. [PubMed: 9382862]
10. Mannella CA, Pfeiffer DR, Bradshaw PC, Moraru II, Slepchenko B, Loew LM, et al. Topology of the mitochondrial inner membrane: dynamics and bioenergetic implications. IUBMB Life. 2001; 52:93–100. [PubMed: 11798041]
11. Lee C, Chen LB. Dynamic behavior of endoplasmic-reticulum in living cells. Cell. 1988; 54:37–46. [PubMed: 3383243]
12. Singer SJ, Nicolson GL. Fluid mosaic model of structure of cell-membranes. Science. 1972; 175:720. [PubMed: 4333397]
13. Canham PB. Minimum energy of bending as a possible explanation of biconcave shape of human red blood cell. J Theor Biol. 1970; 26:61. [PubMed: 5411112]
14. Helfrich W. Elastic properties of lipid bilayers — theory and possible experiments. Z Naturforsch C. 1973; 28:693–703. [PubMed: 4273690]
15. Evans EA. Bending resistance and chemically-induced moments in membrane bilayers. Biophys J. 1974; 14:923–31. [PubMed: 4429770]

16. Deuling HJ, Helfrich W. Red blood-cell shapes as explained on basis of curvature elasticity. Biophys J. 1976; 16:861–8. [PubMed: 938726]
17. Deuling HJ, Helfrich W. Curvature elasticity of fluid membranes — catalog of vesicle shapes. J Phys. 1976; 37:1335–45.
18. Miao L, Seifert U, Wortis M, Dobereiner HG. Budding transitions of fluid-bilayer vesicles — the effect of area-difference elasticity. Phys Rev E. 1994; 49:5389–407.
19. Seifert U. Configurations of fluid membranes and vesicles. Adv Phys. 1997; 46:13–137.
20. Brochard F, Lennon JF. Frequency spectrum of flicker phenomenon in erythrocytes. J Phys. 1975; 36:1035–47.
21. Seifert U, Langer SA. Viscous modes of fluid bilayer-membranes. Europhys Lett. 1993; 23:71–6.
22. Rossier O, Cuvelier D, Borghi N, Puech PH, Derenyi I, Buguin A, et al. Giant vesicles under flows: extrusion and retraction of tubes. Langmuir. 2003; 19:575–84.
23. Peltomäki M, Gompper G. Sedimentation of single red blood cells. Soft Matter. 2013; 9:8346–58.
24. Cowin P, Burke B. Cytoskeleton-membrane interactions. Curr Opin Cell Biol. 1996; 8:56–65. [PubMed: 8791403]
25. Lenz M, Crow DJG, Joanny JF. Membrane buckling induced by curved filaments. Phys Rev Lett. 2009:103.
26. Maugis B, Brugues J, Nassoy P, Guillen N, Sens P, Amblard F. Dynamic instability of the intracellular pressure drives bleb-based motility. J Cell Sci. 2010; 123:3884–92. [PubMed: 20980385]
27. Friedl P, Wolf K. Tumour-cell invasion and migration: diversity and escape mechanisms. Nat Rev Cancer. 2003; 3:362–74. [PubMed: 12724734]
28. Lim FY, Chiam KH, Mahadevan L. The size, shape, and dynamics of cellular blebs. Europhys Lett. 2012:100.
29. Gershfeld NL, Murayama M. Thermal-instability of Red blood-cell membrane bilayers — temperature-dependence of hemolysis. J Membr Biol. 1988; 101:67–72. [PubMed: 3367362]
30. Eskelinen S. Hemolysis of erythrocytes as a model for membrane instability and rupture. J Biol Phys. 1987; 15:22–5.
31. Ginsberg L, Atack JR, Rapoport SI, Gershfeld NL. Regional specificity of membrane instability in Alzheimers-disease brain. Brain Res. 1993; 615:355–7. [PubMed: 8364743]
32. Ginsberg L, Xuereb JH, Gershfeld NL. Membrane instability, plasmalogen content, and Alzheimer's disease. J Neurochem. 1998; 70:2533–8. [PubMed: 9603219]
33. Hatch Emily M, Fischer Andrew H, Deerinck Thomas J, Hetzer Martin W. Catastrophic nuclear envelope collapse in cancer cell micronuclei. Cell. 2013; 154:47–60. [PubMed: 23827674]
34. Leibler S. Curvature instability in membranes. J Phys. 1986; 47:507–16.
35. Edwards DA, Gooch KJ, Zhang I, McKinley GH, Langer R. The nucleation of receptor-mediated endocytosis. Proc Natl Acad Sci U S A. 1996; 93:1786–91. [PubMed: 8700836]
36. Low HH, Sachse C, Amos LA, Lowe J. Structure of a bacterial dynamin-like protein lipid tube provides a mechanism for assembly and membrane curving. Cell. 2009; 139:1342–52. [PubMed: 20064379]
37. Sigismund S, Confalonieri S, Ciliberto A, Polo S, Scita G, Di Fiore PP. Endocytosis and signaling: cell logistics shape the eukaryotic cell plan. Physiol Rev. 2012; 92:273–366. [PubMed: 22298658]
38. Baumgart, T.; Capraro, BR.; Zhu, C.; Das, SL. Thermodynamics and mechanics of membrane curvature generation and sensing by proteins and lipids. In: Leone, SR.; Cremer, PS.; Groves, JT.; Johnson, MA., editors. Annual Review of Physical Chemistry. Vol. 62. 2011. p. 483-506.
39. Taylor MJ, Perrais D, Merrifield CJ. A high precision survey of the molecular dynamics of mammalian clathrin-mediated endocytosis. PLoS Biol. 2011:9.
40. Zilker A, Engelhardt H, Sackmann E. Dynamic reflection interference contrast (ric-) microscopy — a new method to study surface excitations of cells and to measure membrane bending elastic-moduli. J Phys. 1987; 48:2139–51.
41. Betz T, Sykes C. Time resolved membrane fluctuation spectroscopy. Soft Matter. 2012; 8:5317–26.

42. Kononenko VL. Flicker in erythrocytes. I. Theoretical models and registration techniques. Biol Membr. 2009; 26:352–69.
43. Kononenko VL. Flicker in erythrocytes. 2. Review of experimental studies. Biol Membr. 2009; 26:451–67.
44. van Hemmen JL, Leibold C. Elementary excitations of biomembranes: differential geometry of undulations in elastic surfaces. Phys Rep-Rev Sec Phys Lett. 2007; 444:51–99.
45. Zilker A, Ziegler M, Sackmann E. Spectral-analysis of erythrocyte flickering in the 0. 3-4-Mu-M-1 regime by microinterferometry combined with fast image-processing. Phys Rev A. 1992; 46:7998–8002. [PubMed: 9908150]
46. Seifert U, Langer SA. Hydrodynamics of membranes — the bilayer aspect and adhesion. Biophys Chem. 1994; 49:13–22.
47. Kraus M, Seifert U. Relaxation modes of an adhering bilayer-membrane. J Phys II. 1994; 4:1117–34.
48. Divet F, Danker G, Misbah C. Fluctuations and instability of a biological membrane induced by interaction with macromolecules. Phys Rev E. 2005:72.
49. Marchetti MC, Joanny JF, Ramaswamy S, Liverpool TB, Prost J, Rao M, et al. Hydrodynamics of soft active matter. Rev Mod Phys. 2013:85.
50. Helfrich W, Servuss RM. Undulations, Steric Interaction And Cohesion Of Fluid Membranes. Nuovo cimento della societa italiana Di fisica D-condensed matter atomic molecular and chemical. Phys Fluids Plasmas Biophys. 1984; 3:137–51.
51. Seifert U. Dynamics of a bound membrane. Phys Rev E. 1994; 49:3124–7.
52. Lieber AD, Yehudai-Resheff S, Barnhart EL, Theriot JA, Keren K. Membrane tension in rapidly moving cells is determined by cytoskeletal forces. Curr Biol. 2013; 23:1409–17. [PubMed: 23831292]
53. Morris CE, Homann U. Cell surface area regulation and membrane tension. J Membr Biol. 2001; 179:79–102. [PubMed: 11220366]
54. Gov N, Zilman AG, Safran S. Cytoskeleton confinement and tension of red blood cell membranes. Phys Rev Lett. 2003:90.
55. Shkulipa SA, den Otter WK, Briels WJ. Thermal undulations of lipid bilayers relax by intermonolayer friction at submicrometer length scales. Phys Rev Lett. 2006:96.
56. Evans E, Yeung A. Hidden dynamics in rapid changes of bilayer shape. Chem Phys Lipids. 1994; 73:39–56.
57. Rothman JE, Lenard J. Membrane asymmetry. Science. 1977; 195:743–53. [PubMed: 402030]
58. Rahimi M, Arroyo M. Shape dynamics, lipid hydrodynamics, and the complex viscoelasticity of bilayer membranes. Phys Rev E. 2012:86.
59. Merkel R, Sackmann E, Evans E. Molecular friction and epitactic coupling between monolayers in supported bilayers. J Phys. 1989; 50:1535–55.
60. Horner A, Akimov SA, Pohl P. Long and short lipid molecules experience the same interleaflet drag in lipid bilayers. Phys Rev Lett. 2013; 110:268101. [PubMed: 23848924]
61. Rodriguez-Garcia R, Arriaga LR, Mell M, Moleiro LH, Lopez-Montero I, Monroy F. Bimodal spectrum for the curvature fluctuations of bilayer vesicles: pure bending plus hybrid curvature-dilation modes. Phys Rev Lett. 2009:102.
62. Honerkamp-Smith AR, Woodhouse FG, Kantsler V, Goldstein RE. Membrane viscosity determined from shear-driven flow in giant vesicles. Phys Rev Lett. 2013; 111:038103. [PubMed: 23909365]
63. Camley BA, Esposito C, Baumgart T, Brown FLH. Lipid bilayer domain fluctuations as a probe of membrane viscosity. Biophys J. 2010; 99:L44–6. [PubMed: 20858410]
64. Bitbol AF, Puff N, Sakuma Y, Imai M, Fournier JB, Angelova MI. Lipid membrane deformation in response to a local pH modification: theory and experiments. Soft Matter. 2012; 8:6073–82.
65. Bitbol AF, Fournier JB. Membrane properties revealed by spatiotemporal response to a local inhomogeneity. Biochim Biophys Acta Biomembr. 1828; 2013:1241–9.
66. Levin S, Korenstein R. Membrane fluctuations in erythrocytes are linked to mgatp-dependent dynamic assembly of the membrane skeleton. Biophys J. 1991; 60:733–7. [PubMed: 1932557]

67. Staykova M, Holmes DP, Read C, Stone HA. Mechanics of surface area regulation in cells examined with confined lipid membranes. Proc Natl Acad Sci U S A. 2011; 108:9084–8. [PubMed: 21562210]
68. Evans E, Rawicz W. Entropy-driven tension and bending elasticity in condensed-fluid membranes. Phys Rev Lett. 1990; 64:2094–7. [PubMed: 10041575]
69. Brochard F, Degennes PG, Pfeuty P. Surface-tension and deformations of membrane structures — relation to 2-dimensional phase-transitions. J Phys. 1976; 37:1099–104.
70. Borghi N, Rossier O, Brochard-Wyart F. Hydrodynamic extrusion of tubes from giant vesicles. Europhys Lett. 2003; 64:837–43.
71. Tian A, Baumgart T. Sorting of lipids and proteins in membrane curvature gradients. Biophys J. 2009; 96:2676–88. [PubMed: 19348750]
72. Staykova M, Arroyo M, Rahimi M, Stone HA. Confined bilayers passively regulate shape and stress. Phys Rev Lett. 2013:110.
73. Neder J, West B, Nielaba P, Schmid F. Coarse-grained simulations of membranes under tension. J Chem Phys. 2010:132.
74. Milner ST, Safran SA. Dynamical fluctuations of droplet microemulsions and vesicles. Phys Rev A. 1987; 36:4371–9. [PubMed: 9899393]
75. Seifert U. The concept of effective tension for fluctuating vesicles. Z Phys B Condens Matter. 1995; 97:299–309.
76. Girard P, Julicher F, Prost J. Fluid membranes exchanging material with external reservoirs. Eur Phys J E. 2004; 14:387–94. [PubMed: 15340860]
77. Solon J, Pécréaux J, Girard P, Fauré M-C, Prost J, Bassereau P. Negative tension induced by lipid uptake. Phys Rev Lett. 2006; 97:098103. [PubMed: 17026406]
78. Shillcock JC, Lipowsky R. Tension-induced fusion of bilayer membranes and vesicles. Nat Mater. 2005; 4:225–8. [PubMed: 15711550]
79. Sinha B, Koster D, Ruez R, Gonnord P, Bastiani M, Abankwa D, et al. Cells respond to mechanical stress by rapid disassembly of caveolae. Cell. 2011; 144:402–13. [PubMed: 21295700]
80. Masters TA, Pontes B, Viasnoff V, Li Y, Gauthier NC. Plasma membrane tension orchestrates membrane trafficking, cytoskeletal remodeling, and biochemical signaling during phagocytosis. Proc Natl Acad Sci U S A. 2013; 110:11875–80. [PubMed: 23821745]
81. Diz-Munoz A, Fletcher DA, Weiner OD. Use the force: membrane tension as an organizer of cell shape and motility. Trends Cell Biol. 2013; 23:47–53. [PubMed: 23122885]
82. Gauthier NC, Fardin MA, Roca-Cusachs P, Sheetz MP. Temporary increase in plasma membrane tension coordinates the activation of exocytosis and contraction during cell spreading. Proc Natl Acad Sci U S A. 2011; 108:14467–72. [PubMed: 21808040]
83. Gauthier NC, Masters TA, Sheetz MP. Mechanical feedback between membrane tension and dynamics. Trends Cell Biol. 2012; 22:527–35. [PubMed: 22921414]
84. Houk Andrew R, Jilkine A, Mejean Cecile O, Boltyanskiy R, Dufresne Eric R, Angenent Sigurd B, et al. Membrane tension maintains cell polarity by confining signals to the leading edge during neutrophil migration. Cell. 2012; 148:175–88. [PubMed: 22265410]
85. Swift J, Ivanovska IL, Buxboim A, Harada T, Dingal PCDP, Pinter J, et al. Nuclear lamina scales with tissue stiffness and enhances matrix-directed differentiation. Science. 2013:341.
86. Watanabe S, Rost BR, Camacho-Perez M, Davis MW, Sohl-Kielczynski B, Rosenmund C, et al. Ultrafast endocytosis at mouse hippocampal synapses. Nature. 2013; 504:242–7. [PubMed: 24305055]
87. Kabaso D, Shlomovitz R, Schloen K, Stradal T, Gov NS. Theoretical model for cellular shapes driven by protrusive and adhesive forces. PLoS Comput Biol. 2011:7.
88. Tay CY, Cai P, Setyawati MI, Fang W, Tan LP, Hong CHL, et al. Nanoparticles strengthen intracellular tension and retard cellular migration. Nano Lett. 2013; 14:83–8. [PubMed: 24313755]
89. Raucher D, Sheetz MP. Cell spreading and lamellipodial extension rate is regulated by membrane tension. J Cell Biol. 2000; 148:127–36. [PubMed: 10629223]
90. Raucher D, Sheetz MP. Membrane expansion increases endocytosis rate during mitosis. J Cell Biol. 1999; 144:497–506. [PubMed: 9971744]

91. Boulant S, Kural C, Zeeh JC, Ubelmann F, Kirchhausen T. Actin dynamics counteract membrane tension during clathrin-mediated endocytosis. Nat Cell Biol. 2011; 13:1124–U158. [PubMed: 21841790]
92. Li YH, Lipowsky R, Dimova R. Membrane nanotubes induced by aqueous phase separation and stabilized by spontaneous curvature. Proc Natl Acad Sci U S A. 2011; 108:4731–6. [PubMed: 21383120]
93. Lipowsky R. Spontaneous tubulation of membranes and vesicles reveals membrane tension generated by spontaneous curvature. Faraday Discuss. 2013; 161:305–31. [PubMed: 23805747]
94. Domanov YA, Kinnunen PKJ. Antimicrobial peptides temporins B and L induce formation of tubular lipid protrusions from supported phospholipid bilayers. Biophys J. 2006; 91:4427–39. [PubMed: 16997872]
95. Tanaka-Takiguchi Y, Itoh T, Tsujita K, Yamada S, Yanagisawa M, Fujiwara K, et al. Physicochemical analysis from real-time imaging of liposome tubulation reveals the characteristics of individual F-BAR domain proteins. Langmuir. 2012; 29:328–36. [PubMed: 23199228]
96. Barziv R, Moses E. Instability and pearling states produced in tubular membranes by competition of curvature and tension. Phys Rev Lett. 1994; 73:1392–5. [PubMed: 10056781]
97. Nelson P, Powers T, Seifert U. Dynamical theory of the pearling instability in cylindrical vesicles. Phys Rev Lett. 1995; 74:3384–7. [PubMed: 10058187]
98. Yu Y, Granick S. Pearling of lipid vesicles induced by nanoparticles. J Am Chem Soc. 2009; 131:14158. [PubMed: 19775107]
99. Tsafrir I, Caspi Y, Guedeau-Boudeville MA, Arzi T, Stavans J. Budding and tubulation in highly oblate vesicles by anchored amphiphilic molecules. Phys Rev Lett. 2003:91.
100. Kas J, Sackmann E. Shape transitions and shape stability of giant phospholipid-vesicles in pure water induced by area-to-volume changes. Biophys J. 1991; 60:825–44. [PubMed: 1742455]
101. Jaric M, Seifert U, Wintz W, Wortis M. Vesicular instabilities — the prolate-to-oblate transition and other shape instabilities of fluid bilayer-membranes. Phys Rev E. 1995; 52:6623–34.
102. Kumar PBS, Rao M. Shape instabilities in the dynamics of a two-component fluid membrane. Phys Rev Lett. 1998; 80:2489–92.
103. Seifert U. Curvature-induced lateral phase segregation in 2-component vesicles. Phys Rev Lett. 1993; 70:1335–8. [PubMed: 10054350]
104. Sheetz MP, Singer SJ. Biological-membranes as bilayer couples — molecular mechanism of drug-erythrocyte interactions. Proc Natl Acad Sci U S A. 1974; 71:4457–61. [PubMed: 4530994]
105. Campelo F. Modeling morphological instabilities in lipid membranes with anchored amphiphilic polymers. J Chem Biol. 2009; 2:65–80. [PubMed: 19568784]
106. Berndl K, Kas J, Lipowsky R, Sackmann E, Seifert U. Shape transformations of giant vesicles — extreme sensitivity to bilayer asymmetry. Europhys Lett. 1990; 13:659–64.
107. Seifert U, Berndl K, Lipowsky R. Shape transformations of vesicles — phase-diagram for spontaneous-curvature and bilayer-coupling models. Phys Rev A. 1991; 44:1182–202. [PubMed: 9906067]
108. Seul M, Andelman D. Domain shapes and patterns — the phenomenology of modulated phases. Science. 1995; 267:476–83. [PubMed: 17788780]
109. Zhu C, Das SL, Baumgart T. Nonlinear sorting, curvature generation, and crowding of endophilin N-BAR on tubular membranes. Biophys J. 2012; 102:1837–45. [PubMed: 22768939]
110. Cahn JW, Hilliard JE. Free energy of a nonuniform system .1. Interfacial free energy. J Chem Phys. 1958; 28:258–67.
111. Fournier JB. Nontopological saddle-splay and curvature instabilities from anisotropic membrane inclusions. Phys Rev Lett. 1996; 76:4436–9. [PubMed: 10061289]
112. Kabaso D, Bobrovska N, Gozdz W, Gov N, Kralj-Iglic V, Veranic P, et al. On the role of membrane anisotropy and BAR proteins in the stability of tubular membrane structures. J Biomech. 2012; 45:231–8. [PubMed: 22138195]
113. Loew S, Hinderliter A, May S. Stability of protein-decorated mixed lipid membranes: the interplay of lipid–lipid, lipid–protein, and protein–protein interactions. J Chem Phys. 2009:130.

114. Veksler A, Gov NS. Phase transitions of the coupled membrane-cytoskeleton modify cellular shape. Biophys J. 2007; 93:3798–810. [PubMed: 17704150]
115. Chiruvolu S, Warriner HE, Naranjo E, Idziak SHJ, Radler JO, Plano RJ, et al. A phase of liposomes with entangled tubular vesicles. Science. 1994; 266:1222–5. [PubMed: 7973704]
116. Allan D, Billah MM, Finean JB, Michell RH. Release of diacylglycerol-enriched vesicles from erythrocytes with increased intracellular Ca2 + Nature. 1976; 261:58–60. [PubMed: 775341]
117. Leirer C, Wunderlich B, Myles VM, Schneider MF. Phase transition induced fission in lipid vesicles. Biophys Chem. 2009; 143:106–9. [PubMed: 19442430]
118. Kabaso D, Shlomovitz R, Auth T, Lew VL, Gov NS. Curling and local shape changes of Red blood cell membranes driven by cytoskeletal reorganization. Biophys J. 2010; 99:808–16. [PubMed: 20682258]
119. Leibler S, Andelman D. Ordered and curved meso-structures in membranes and amphiphilic films. J Phys. 1987; 48:2013–8.
120. Santangelo CD, Farago O. Membrane fluctuations around inclusions. J Comput Aided Mater Des. 2007; 14:103–9.
121. Hu JG, Granek R. Buckling of amphiphilic monolayers induced by head-tail asymmetry. J Phys II. 1996; 6:999–1022.
122. Lipp MM, Lee KYC, Takamoto DY, Zasadzinski JA, Waring AJ. Coexistence of buckled and flat monolayers. Phys Rev Lett. 1998; 81:1650–3.
123. Bourdieu L, Daillant J, Chatenay D, Braslau A, Colson D. Buckling of polymerized monomolecular films. Phys Rev Lett. 1994; 72:1502–5. [PubMed: 10055625]
124. Kardar M, Golestanian R. The “friction” of vacuum, and other fluctuation-induced forces. Rev Mod Phys. 1999; 71:1233–45.
125. Benhamou M. Primitive interactions between inclusions on a fluid membrane: the role of thermal fluctuations. Eur Phys J E. 2011:34.
126. Lin HK, Zandi R, Mohideen U, Pryadko LP. Fluctuation-induced forces between inclusions in a fluid membrane under tension. Phys Rev Lett. 2011:107.
127. Goulian M, Bruinsma R, Pincus P. Long-range forces in heterogeneous fluid membranes. Europhys Lett. 1993; 22:145–50.
128. Yolcu C, Deserno M. Membrane-mediated interactions between rigid inclusions: an effective field theory. Phys Rev E. 2012:86.
129. Demery V. Diffusion of a particle quadratically coupled to a thermally fluctuating field. Phys Rev E. 2013:87.
130. Manneville JB, Bassereau P, Ramaswamy S, Prost J. Active membrane fluctuations studied by micropipet aspiration. Phys Rev E. 2001:64.
131. Loubet B, Seifert U, Lomholt MA. Effective tension and fluctuations in active membranes. Phys Rev E. 2012:85.
132. Koltover I, Radler JO, Safinya CR. Membrane mediated attraction and ordered aggregation of colloidal particles bound to giant phospholipid vesicles. Phys Rev Lett. 1999; 82:1991–4.
133. Morozova D, Guigas G, Weiss M. Dynamic structure formation of peripheral membrane proteins. PLoS Comput Biol. 2011:7.
134. Ramakrishnan N, Sunil Kumar PB, Ipsen John H. Membrane-mediated aggregation of curvature-inducing nematogens and membrane tubulation. Biophys J. 2013; 104:1018–28. [PubMed: 23473484]
135. Weitz S, Destainville N. Attractive asymmetric inclusions in elastic membranes under tension: cluster phases and membrane invaginations. Soft Matter. 2013; 9:7804–16.
136. Gil T, Ipsen JH, Mouritsen OG, Sabra MC, Sperotto MM, Zuckermann MJ. Theoretical analysis of protein organization in lipid membranes. Biochim Biophys Acta. 1998; 1376:245–66. [PubMed: 9804966]
137. Morozova D, Weiss M, Guigas G. Shape as a determinant of membrane protein cluster formation. Soft Matter. 2012; 8:11905–10.
138. Ramanan V, Agrawal NJ, Liu J, Engles S, Toy R, Radhakrishnan R. Systems biology and physical biology of clathrin-mediated endocytosis. Integr Biol. 2011; 3:803–15.

139. Cocucci E, Aguet F, Boulant S, Kirchhausen T. The first five seconds in the life of a clathrin-coated pit. Cell. 2012; 150:495–507. [PubMed: 22863004]
140. Kukulski W, Schorb M, Kaksonen M, Briggs JAG. Plasma membrane reshaping during endocytosis is revealed by time-resolved electron tomography. Cell. 2012; 150:508–20. [PubMed: 22863005]
141. Idrissi F-Z, Blasco A, Espinal A, Geli MI. Ultrastructural dynamics of proteins involved in endocytic budding. Proc Natl Acad Sci. 2012; 109:E2587–94. [PubMed: 22949647]
142. McGough IJ, Cullen PJ. Clathrin is not required for SNX-BAR-retromer mediated carrier formation. J Cell Sci. 2012; 126:45–52. [PubMed: 23015596]
143. Mim C, Cui HS, Gawronski-Salerno JA, Frost A, Lyman E, Voth GA, et al. Structural basis of membrane bending by the N-BAR protein endophilin. Cell. 2012; 149:137–45. [PubMed: 22464326]
144. Frost A, Perera R, Roux A, Spasov K, Destaing O, Egelman EH, et al. Structural basis of membrane invagination by F-BAR domains. Cell. 2008; 132:807–17. [PubMed: 18329367]
145. Hom RA, Vora M, Regner M, Subach OM, Cho W, Verkhusha VV, et al. PH-dependent binding of the epsin ENTH domain and the AP180 ANTH domain to PI(4,5)P-2-containing bilayers. J Mol Biol. 2007; 373:412–23. [PubMed: 17825837]
146. Yoon Y, Zhang X, Cho W. Phosphatidylinositol 4,5-bisphosphate (PtdIns(4,5)P2) specifically induces membrane penetration and deformation by bin/amphiphysin/rvs (BAR) domains. J Biol Chem. 2012; 287:34078–90. [PubMed: 22888025]
147. Capraro BR, Shi Z, Wu T, Chen Z, Dunn JM, Rhoades E, et al. Kinetics of endophilin N-BAR domain dimerization and membrane interactions. J Biol Chem. 2013; 288:12533–43. [PubMed: 23482561]
148. Cui H, Mim C, Vázquez Francisco X, Lyman E, Unger Vinzenz M, Voth Gregory A. Understanding the role of amphipathic helices in N-BAR domain driven membrane remodeling. Biophys J. 2013; 104:404–11. [PubMed: 23442862]
149. Simunovic M, Srivastava A, Voth GA. Linear aggregation of proteins on the membrane as a prelude to membrane remodeling. Proc Natl Acad Sci. 2013; 110:20396–401. [PubMed: 24284177]
150. Sorre B, Callan-Jones A, Manzi J, Goud B, Prost J, Bassereau P, et al. Nature of curvature coupling of amphiphysin with membranes depends on its bound density. Proc Natl Acad Sci U S A. 2012; 109:173–8. [PubMed: 22184226]
151. Atilgan E, Sun SX. Shape transitions in lipid membranes and protein mediated vesicle fusion and fission. J Chem Phys. 2007:126.
152. Gozdz WT. Shape transformation of lipid vesicles induced by diffusing macromolecules. J Chem Phys. 2011:134.
153. Simunovic M, Mim C, Marlovits TC, Resch G, Unger VM, Voth GA. Protein-mediated transformation of lipid vesicles into tubular networks. Biophys J. 2013; 105:711–9. [PubMed: 23931319]
154. Meinecke M, Boucrot E, Camdere G, Hon WC, Mittal R, McMahon HT. Cooperative recruitment of dynamin and BIN/amphiphysin/Rvs (BAR) domain-containing proteins leads to GTP-dependent membrane scission. J Biol Chem. 2013; 288:6651–61. [PubMed: 23297414]
155. Minton AP. Effects of excluded surface area and adsorbate clustering on surface adsorption of proteins. II. Kinetic models. Biophys J. 2001; 80:1641–8. [PubMed: 11259279]
156. Frost A, Unger VM, De Camilli P. The BAR domain superfamily: membrane-molding macromolecules. Cell. 2009; 137:191–6. [PubMed: 19379681]
157. Xu P, Baldridge RD, Chi RJ, Burd CG, Graham TR. Phosphatidylserine flipping enhances membrane curvature and negative charge required for vesicular transport. J Cell Biol. 2013; 202:875–86. [PubMed: 24019533]
158. Ouberai MM, Wang J, Swann MJ, Galvagnion C, Guilliams T, Dobson CM, et al. Alpha-synuclein senses lipid packing defects and induces lateral expansion of lipids leading to membrane remodeling. J Biol Chem. 2013; 288:20883–95. [PubMed: 23740253]
159. Cui HS, Lyman E, Voth GA. Mechanism of membrane curvature sensing by amphipathic helix containing proteins. Biophys J. 2011; 100:1271–9. [PubMed: 21354400]

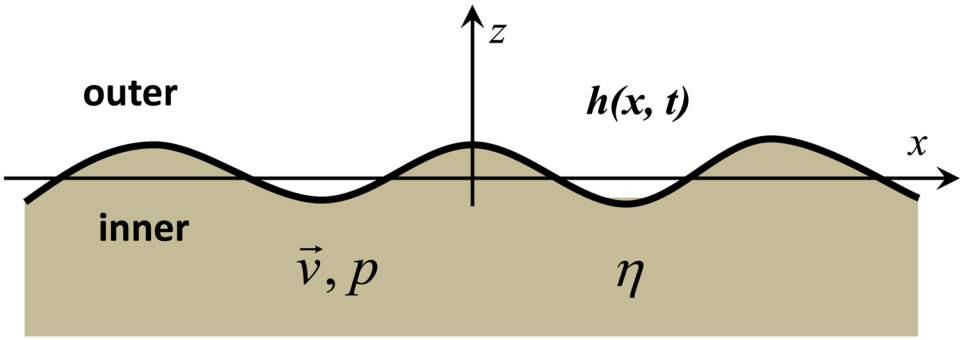

Fig. 1.
Sketch of a fluctuating membrane (black curve) in liquid environment (gray).

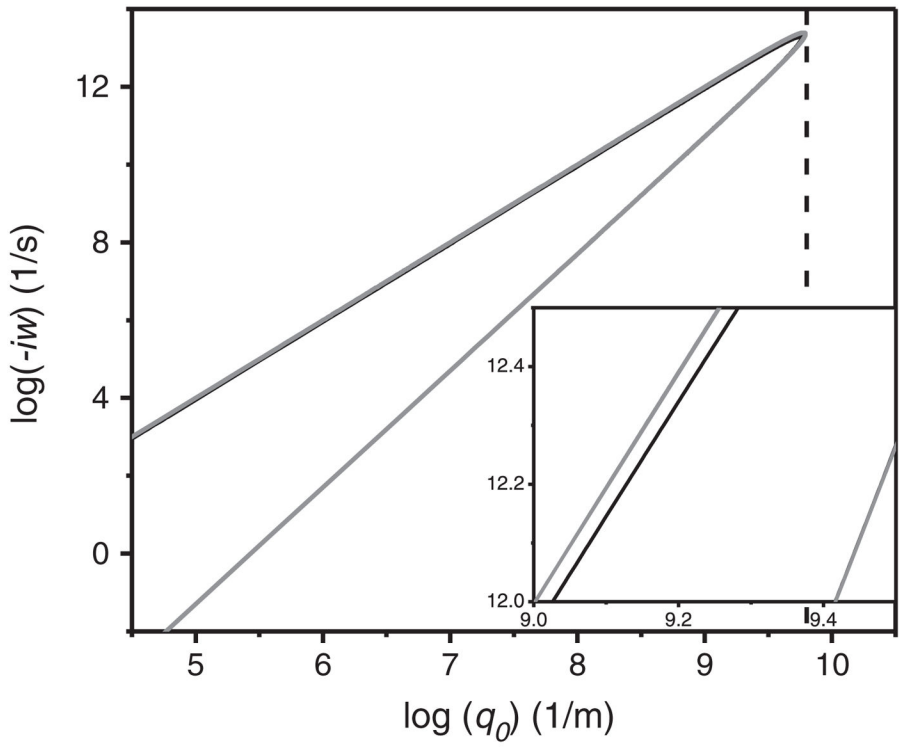

Fig. 2.

A comparison of the two dispersion relations resulting from Eqs. (9′) (black) and (9″) (gray) respectively. As can be seen in the figure, the slow modes (lower part) of two dispersion relations are indistinguishable (overlapped). However, the fast mode (upper part) shows a difference (as becomes clear in the zoomed-in figure of the inset) between two dispersion relations. $\kappa = 10^{-19}$ J, $\rho = 10^3$ kg/m^3, $\eta = 10^{-3}$ J s/m^3 were used for the plot and the dashed line represents the corresponding value for $\log(q_0^*)$.

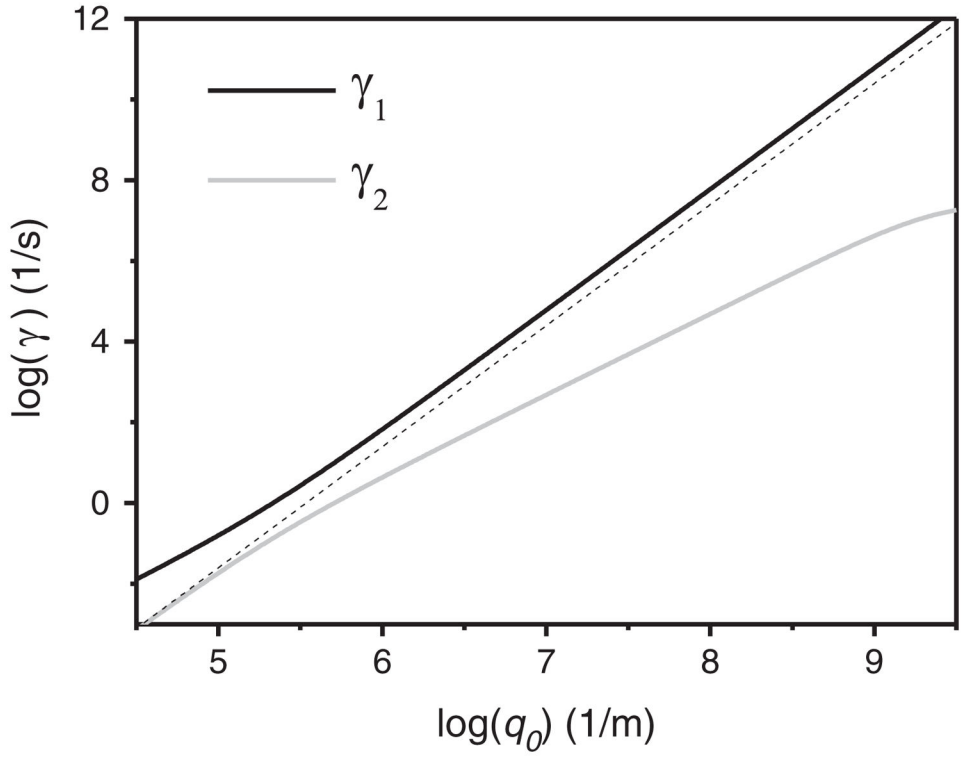

Fig. 3.

Dispersion relation for a single bilayer membrane with interleaflet damping. The black and gray solid lines are the fast and slow viscous modes respectively. The dotted line represents the conventional bending mode: $\gamma = \kappa q_0^3 / 4\eta$ (adapted from Fig. 2 of [21], $\kappa = 10^{-19}$ J, k = 0.07 J/m^2, $d = 10^{-9}$ m, $\eta = 10^{-3}$ J s/m^3, $\mu = 10^{-9}$ J s/m^2, $b_f = 3 \times 10^9$ J s/m^4 are used for the plot).

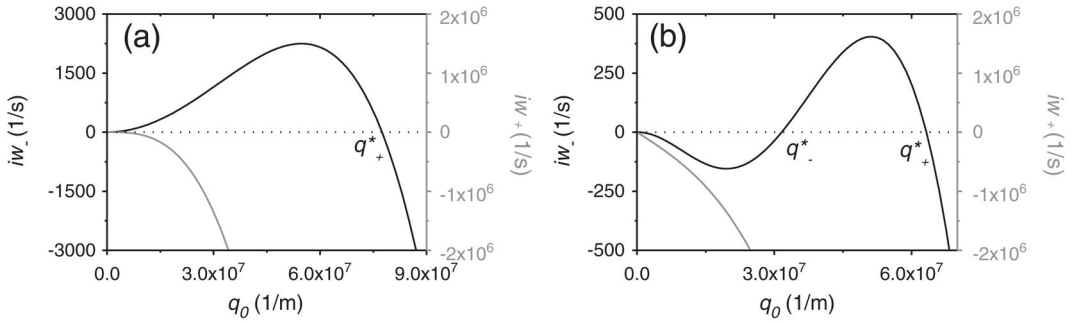

Fig. 4.

iw as a function of q_0, the planar membrane is stable when $iw < 0$. Membrane tension $\sigma = 0$ in Figure (a) and $\sigma = 10^{-4}$ N/m in Figure (b). The black lines represent the 'iw_-' branch, the gray lines represent the 'iw_+' branch, the dotted lines are $iw = 0$. As shown, 'iw_+' is always negative while 'iw_-' is positive for $0 < q_0 < q^*_+$ in (a) and for $q^*_- < q_0 < q^*_+$ in (b). It can be seen that the presence of membrane tension lowers the range and amplitude of the unstable ($iw>0$) regime. ($\kappa = 10^{-19}$ J, $\eta = 10^{-3}$ J s/m^3, $D = 10^{-12}$ m^2/s, $a_{eff} = 4 \times 10^{-4}$ N/m, $b = 10^{-19}$ J, $C_0 = 10^8$ m^{-1} were used for the plots).